August 1998

Request for SLD Run Extension

SLD Collaboration
Stanford Linear Accelerator Center, Stanford University, Stanford, CA 94309

Contents

Part I
Overview

We are proposing an extension of the SLD running at the SLC beyond the end of the present 1997-98 run. The goal of such an extension is to bring the total accumulated polarized Z's with the new vertex detector VXD3 up to a million. The record breaking performance of the SLC in the Spring of 1998 makes us believe that this goal is realistic. We also believe that the physics results that can be obtained from such a sample of polarized Z's will be unique. It will provide the most precise measurements, and therefore crucial insights, on several topics which are at the very heart of the Standard Model. The features of SLD/SLC that allow such compelling physics results, i.e. highly polarized electron beams, unparalleled vertex detection and particle identification, do not exist at any other facility in the world, and are not likely to exist again in the foreseeable future after the closedown of the SLD/SLC program. It therefore seems to us that the modest additional effort and resources required to allow this program to achieve its natural potential is well justified, considering the importance of the physics results and the large investment the community has already made in this project.

Foremost among the measurements that can be made with such a large sample of polarized Z's is the most precise measurement in the world of $\sin^2\theta_W^{\rm eff}$, the electroweak mixing angle, via the measurement of A_{LR}, the left-right polarization asymmetry. This measurement is by far the most powerful way to measure this crucial parameter, and requires polarized incident electrons and is thus unique to SLD/SLC. At the present time, the precision on $\sin^2\theta_W^{\rm eff}$ from this single measurement is comparable to the combined result of the measurement of six different parameters in each of four experiments at LEP. There is an intriguing 2.2 standard deviation discrepancy between these results. It may be worth pointing out that the A_{LR} measurement depends only on the Z coupling to electrons, while the most precise LEP measurements involve couplings to hadrons, with a larger inherent uncertainty in interpretation. This difference while seemingly small, leads to two quite different conclusions about the nature of the electroweak symmetry breaking in the Standard Model which is, itself, an issue of central importance in our field. A significant improvement in the precision of this measurement thus is of primary importance at this time. With the precision of ± 0.00018 in $\sin^2\theta_W^{\rm eff}$ that we can obtain with this extended SLD/SLC run we will be able to pinpoint the Higgs mass to a fairly narrow range, or, depending on the exact value of $\sin^2\theta_W^{\rm eff}$, rule out the single standard model Higgs as the source of the electroweak symmetry breaking. As pointed out above, there is no alternate opportunity in the foreseeable future in the world to carry out this measurement once the SLD/SLC program is terminated.

A second area where SLD would make a unique and important contribution is in the study of mixing in the B_s^0 system. Since the B_s^0-$\bar{B}_s^0$ oscillation is expected to have a high frequency, the unparalleled resolution of the SLD vertex detector VXD3 will provide unique sensitivity to larger mass differences (Δm_s). This, combined with the highly efficient and pure initial state tag provided by the polarized electron beam and the large b-quark forward-backward asymmetry, and the superior final state tags provided by the vertex detector and good particle ID in the CRID, will allow SLD to probe a region well beyond that reachable by existing experiments. With a sample of a million polarized Z events, SLD should be able to convincingly measure the B_s^0 mixing frequency up to $\Delta m_s \sim 15$ ps^{-1} or to rule out mixing frequencies up to $\Delta m_s \sim 20$ ps^{-1} at the 95% confidence level. Since best present information predicts that Δm_s is in the range 8 ps^{-1}-16 ps^{-1} and the current 95% limit from LEP is $\Delta m_s > 11.5$ ps^{-1}, the region of SLD sensitivity is very significant. A first measurement of Δm_s would provide a determination of the least well known CKM matrix element $|V_{td}|$ and would determine the unitarity triangle via the measurement of its sides. Combined with determinations of the interior angles from measurements of CP violating processes at the next generation of B-factories, this information will overdetermine the unitarity triangle and will provide insight into the relationship between the CKM matrix and CP violation.

Another example of an important and unique b-quark result would be the measurement of the asymmetry A_b in the Z to b-quark couplings. SLD is unique in being able to measure this quantity directly. Without polarized beams, only the product of the b quark and the electron couplings can be measured complicating the interpretation of the result. A most precise in the world measurement of this quantity with a million polarized Z events is important for two reasons. It provides a sensitive test of new physics from vertex corrections at the $Zb\bar{b}$ vertex (it is particularly sensitive to processes which affect the right-handed coupling) and a precise value of A_b plays an important role in interpreting the precise measurements of the unpolarized b-quark forward-backward asymmetry performed by the LEP Collaborations.

While the left-right polarization asymmetry, B_s mixing parameter, and b-quark asymmetry measurements are the compelling reasons for the run extension, the unique capabilities of SLD/SLC will lead to unique and significant measurements in QCD. This is particularly clear where heavy quark identification is important, such as fundamental measurements in b-bbar gluon decays and gluon splitting to b-bbar and c-cbar quark pairs.

Part II
SLC Luminosity Expectations

The goal of this Request for Extension is to accumulate a sample of approximately one million Z events with VXD3. This implies that an additional sample of 650,000 events would be logged during the extended running. The 650K event goal can be achieved via several luminosity/running time scenarios. The performance of the SLC during the 1998 run and the experience of running with the PEP-II commissioning program indicates that a rate of 15K events/week (after an SLC startup period) is a reasonably conservative expectation. In this scenario, a run of 40 weeks after a startup period would be sufficient to achieve the goal. However, it also appears that a very modest program of accelerator improvements would significantly increase the SLC luminosity. The improved luminosity could be used to achieve the integrated event total in a shorter, cheaper run or to exceed the 650K event goal in a 40 week run. The SLD Collaboration would be delighted by either prospect!

The current run began in June of 1997 with an extended turn-on and recommissioning period. A deliberate decision was made to dedicate substantial time to machine physics.

While the accelerator physics progress was promising, the machine reliability was a problem. Beginning in October of 1997, the machine improved and an average event rate of more than 10K Z's per week was sustained until the December shutdown. During this period, there were two weeks that exceeded 14k Z events logged. Although the average luminosity decreased somewhat after the Christmas/New Year shutdown, the luminosity improvement slope was maintained. By the end of March, a sequence of record shifts and days resulted in an unprecedented week of 17,000 Z's. This was followed two weeks later by a week of 21,000 Z's. This performance is shown in Figure 1.

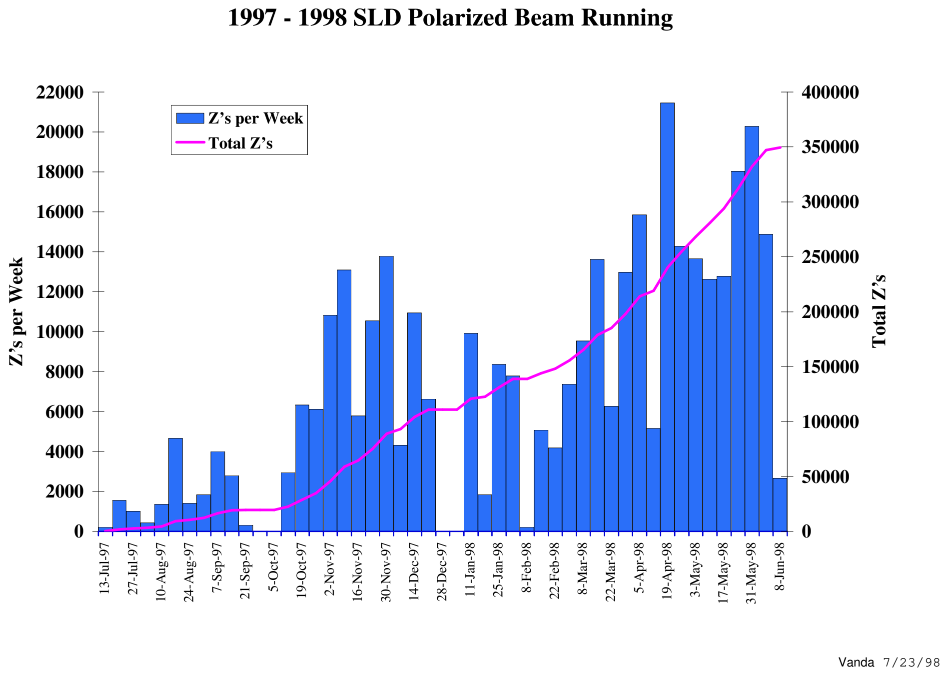

Figure 1: The number of Z events logged per week during the 1997-98 run. The integral is shown as the solid curve.

The series of small improvements continued throughout the spring of 1998 and by the beginning of June, the SLC achieved periods of more than 250 Z's/hour operation (measured with SLD Z and Bhabha event rates). As is shown in Fig. 2, operation at more than 200 Z's/hour was frequent during this period. The machine availability was typically 100 hours per week during the post October 1997 running. Using this number with the demonstrated luminosity and a 15-20% inefficiency from combined PEP-II/SLC operation leads to the 15K Z events/week estimate given above.

The luminosity increase in the 1997-98 run was largely due to increased demagnification in the final focus, decreased beam emittance (due to improved tuning procedures for beam-based alignment, steering, and emittance control), and the onset of significant pinch-enhancement (up to a 100% effect). The tuning of the linac orbit bumps that cancel wakefield tails is now based upon emittance measurements made in the final focus rather than mea-

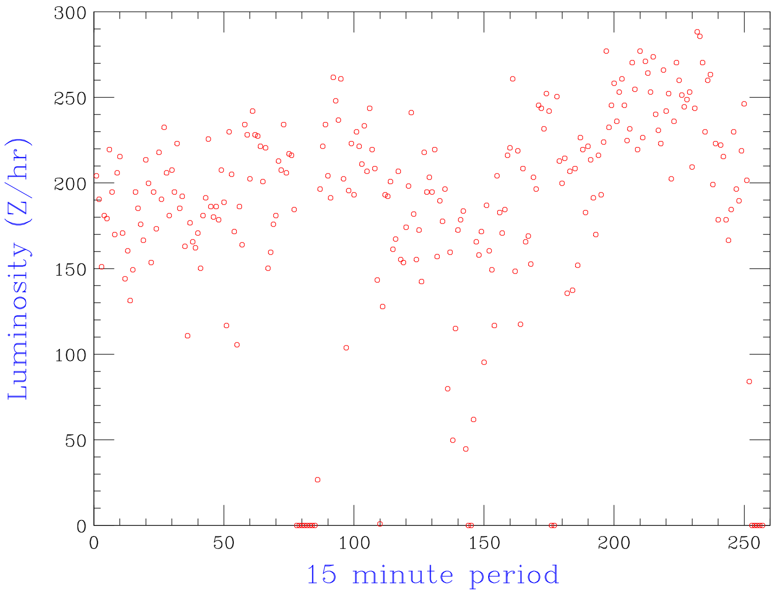

Figure 2: The average number of Z's per hour measured by the SLD luminosity monitor of Bhabha events combined with detected Z events as measured during the last 2.5 days of the 1998 run. Each entry in the histogram represents a 15 minute period.

surements made at the end of the linac (accounts for effects occurring at the end of the linac). A new technique for final focus tuning based upon the dithering of 10 critical parameters was estimated to deliver about 30% more luminosity. A number of small hardware improvements also contributed to the luminosity increase. Wakefield emittance growth in the Ring-To-Linac transport lines was decreased by the installation of shielding sleeves in the vacuum bellows. Octupoles were installed in the chromatic correction sections of the final focus regions to cancel third-order aberrations at the interaction point (IP). The strengths of the Q1's, the quadrupoles closest to the IP, were increased to decrease the IP beta function. These improvements which contributed to the performance of the SLC (particularly in 1998) form the basis of the upgrade program for the next run (see the accompanying document). It is believed that the upgraded SLC would (very conservatively) achieve an average luminosity exceeding 20K Z events per week.

Part III
The SLD Detector

1 Introduction

The SLD detector brings together a unique combination of tools perfectly suited to precision measurements of electroweak parameters, B mixing, and heavy flavor QCD. The collisions of highly polarized electrons with unpolarized positrons produce the fundamental rate and angular asymmetries that are used to measure the fundamental electroweak parameters. SLD's Compton Polarimeter measures the electron polarization precisely and continuously and thus sets the scale for nearly all the electroweak measurements. SLD's CCD vertex detector, in conjunction with the main tracking chamber, provides the highest resolution vertex reconstruction in the world today, and identifies heavy quarks with unparalleled efficiency. The SLD CRID identifies hadronic particles efficiently over a wide momentum range with low misidentification rate. The identification of charged kaons among the heavy quark decay products flavor tags the decays. Used all together, as they are for example in the B_s mixing measurements, these tools afford SLD unique measurement capability.

2 Polarimeter

The Compton polarimeter [1] shown in Figure 3, detects both Compton-scattered electrons and Compton-backscattered gammas from the collision of the longitudinally polarized 45.6 GeV electron beam [2] with a circularly polarized photon beam. After the Compton Interaction Point (CIP), the electrons and backscattered gammas pass through a dipole spectrometer. A nine-channel threshold Cherenkov detector (CKV) measures electrons in the range 17 to 30 GeV.* Two detectors, a single-channel Polarized Gamma Counter (PGC) [3] and a multi-channel Quartz Fiber Calorimeter (QFC) [4], are located in the neutral beamline to measure the counting rates of the Compton-scattered gammas.

The CKV detector is the only one of these detectors which can make polarization measurements during beam collisions. Hence, it is the primary detector and the most carefully analyzed. A summary of the systematic errors associated with its polarization measurement is given in Table 1. The error noted for the SLC IP vs Compton IP reflects that the luminosity-weighted polarization at the SLC IP can differ from the average polarization measured at the Compton IP. This includes the effects of depolarization from the beam-beam interaction, chromatic effects, and steering effects [2]. Analysis of data from the PGC and QFC detectors is not yet complete, but preliminary results are consistent with the CKV result to within 1%. Typical beam polarizations for the SLD experiment have been in the range $73 - 77\%$. With some modest upgrades, we expect to achieve a systematic error on the polarization measurement at or below the 0.5% level.

*The kinematic edge with maximal asymmetry is at an electron energy of 17.4 GeV, and the zero-asymmetry point is at 25.2 GeV.

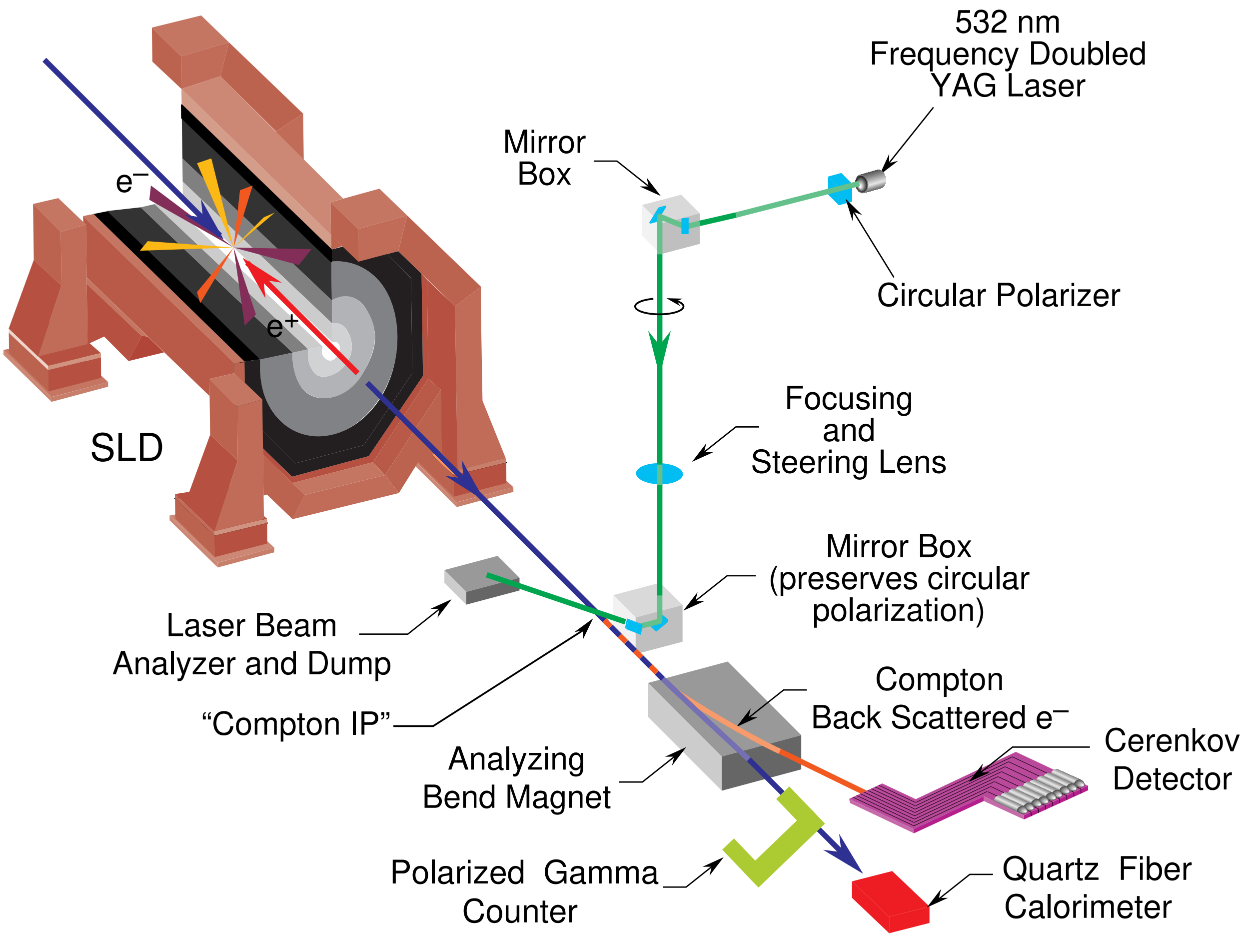

Figure 3: Compton Polarimeter for the SLD Experiment

Table 1: Systematic Errors for CKV Polarization Measurement

Item	Error
Analyzing Power	0.3%
Detector Linearity	0.5%
Electronics Linearity	0.2%
Laser Polarization	0.2%
SLC IP vs Compton IP	0.2%
Total	0.7%

3 Tracking and Vertexing

The upgrade vertex detector VXD3 is extremely reliable and well tuned, though there were two significant deficiencies in its first year of operation (1996): electronics failures and radiation damage. The electronics failures were a mix of operational problems, *in situ* failures, and one general problem (inadequate cooling) that exacerbated the other difficulties. All these problems were addressed and corrected after the 1996 run, and the electronics has operated extremely reliably ever since. The radiation damage to the CCDs (particularly the inward facing devices on layer 1) occurred during a period of non-standard SLC operation before the start of the 1996 run. This caused a significant loss of efficiency for large negative $\cos\theta$. Once this effect was understood, it was completely cured by operating the detector at a lower temperature (183 K in the 1997-98 run compared with 220 K in the 1996 run). See Fig. 4 for a comparison between the 1996 and 1997 performance. For the Central Drift Chamber (CDC), a broken wire represented the only significant failure. Here, it emerged that the wire had been damaged before the initial assembly of the chamber, so this failure should not be seen as the onset of some aging problem.

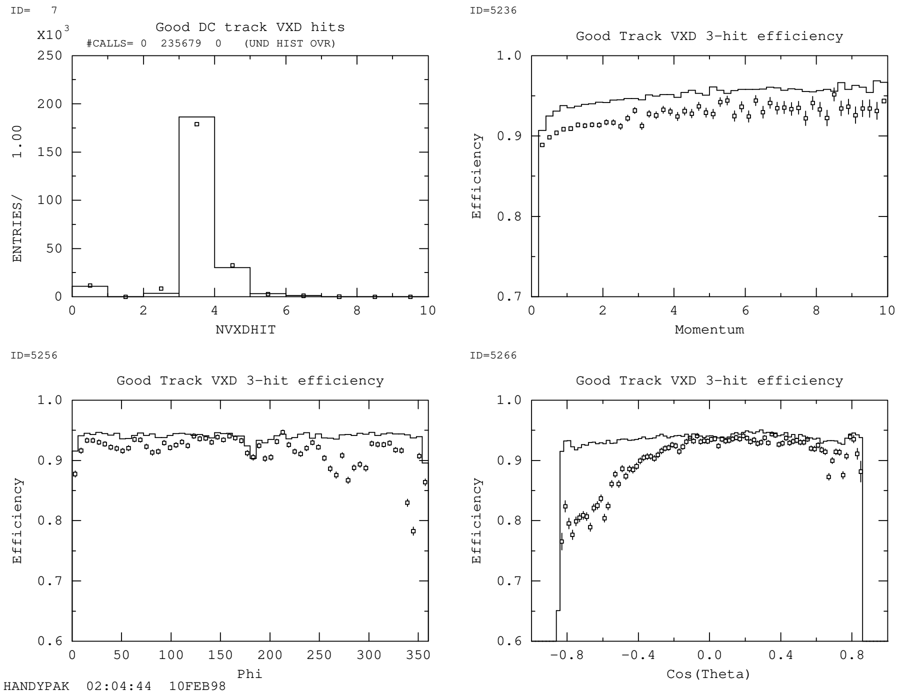

Figure 4: Distributions of the number of VXD hits per track and 3-hit linking efficiency as functions of momentum, azimuthal angle, and $\cos\theta$ for 1996 data (points) and 1997 data (histograms).

Following the track based internal alignment of the vertex detector, the impact parameter precision as a function of momentum (Fig. 5) is about a factor two better than with

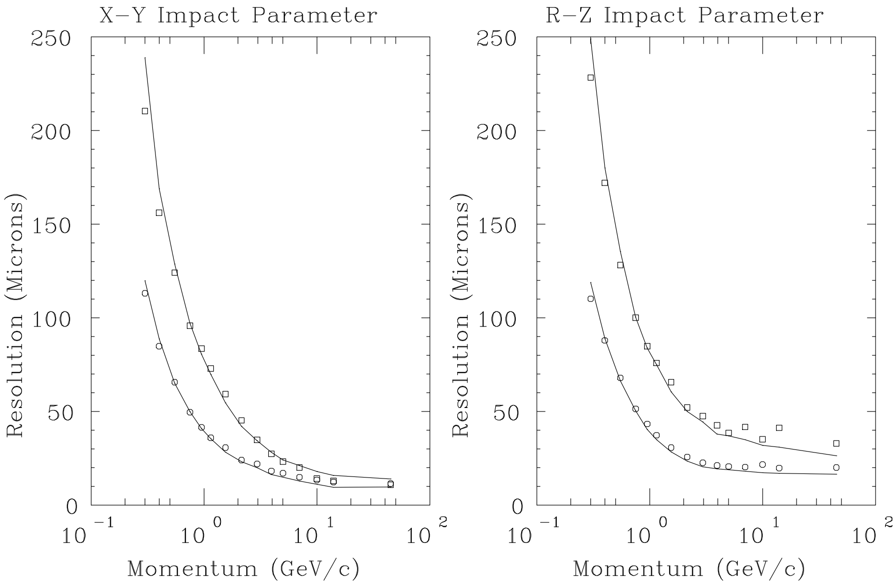

Figure 5: Impact parameter resolution as a function of momentum for VXD2 data (square points) VXD3 1996 data (circle points) with the corresponding Monte Carlo curves.

SLD's original vertex detector over the full momentum range. As a result of the improvements in the 1997 performance of the vertex detector, together with a larger data sample from high luminosity running, it has been possible to carry out an even more robust and accurate internal alignment than in 1996. All local residual distributions have been reduced to correspond to intrinsic hit resolution below 5 μm. Furthermore, muon pair data indicate impact parameter precision at the IP of 10.7 μm (xy) and 11.4 μm (rz) for tracks fitted using the VXD3 hits alone; see Fig. 6. These results demonstrate that VXD3 is now operating at its design performance.

Since 1995, SLD has broken new ground in terms of vertex finding, and the physics analyses that flow from this work. The breakthrough came from a robust *topological* vertex finding procedure, in which (as far as possible) one finds any secondary vertices in a jet, and unambiguously associates the charged tracks with those vertices. This procedure is given a very strong start in SLD by the fact that the primary vertex for any event is measured in $r\phi$ with high precision $\sim 7\mu$m ($\sim$ 5 μm for 1998) by averaging over sets of $\sim$ 30 events. The z location of the primary vertex is found on an event by event basis to within $\sim 20\mu$m.

The quality of the topological vertexing has been refined to the point where it is a very powerful physics tool. It forms the basis of the technique used to tag b and c hadrons. For tagging b hadrons, all the well-measured tracks are used to search for secondary vertices by identifying regions of high track overlap density in 3-D coordinate space. Individual tracks are represented as Gaussian probability tubes whose width represents the impact parameter error. A secondary vertex clearly separated from the known interaction point serves as a seed to which other tracks in the event are attached if they are more likely to have originated

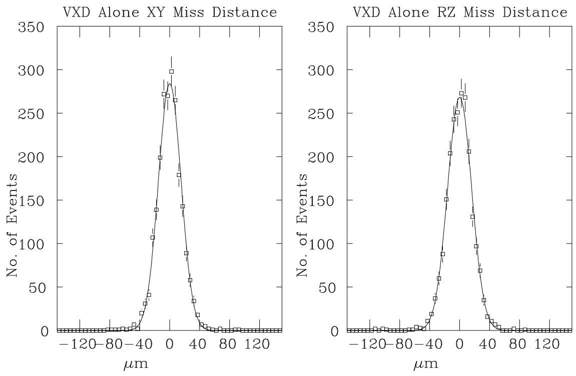

Figure 6: Mu pair miss-distance using VXD3 hits only for the 1997 data

in the heavy quark decay than in the primary interaction. The invariant mass of these tracks, augmented by the missing momentum inferred from the mismatch of the vertex momentum vector and the observed decay direction, serves to distinguish charm from b decays as shown in Figure 7. The resulting b tag is remarkably background free, and highly efficient (see Figure 8). A similar technique serves to identify charm decays topologically. In this case, one chooses intermediate vertex masses, which are roughly half-b and half-c. The b contamination is reduced by noting that the net momentum of the secondary tracks is higher for charm decays than for b's, as shown in Figure 9. The charm tag has an efficiency of 14% and a purity of 67%, which sets an industry standard.

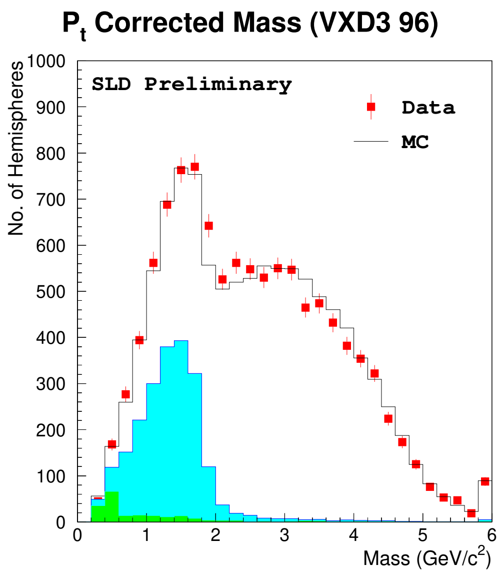

Figure 7: The P_t corrected mass of tracks associated with secondary vertices in Z decays.

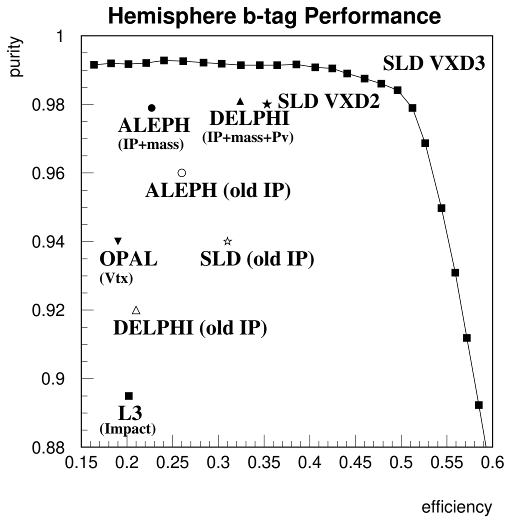

Figure 8: Efficiency vs Purity for b tags from various experiments.

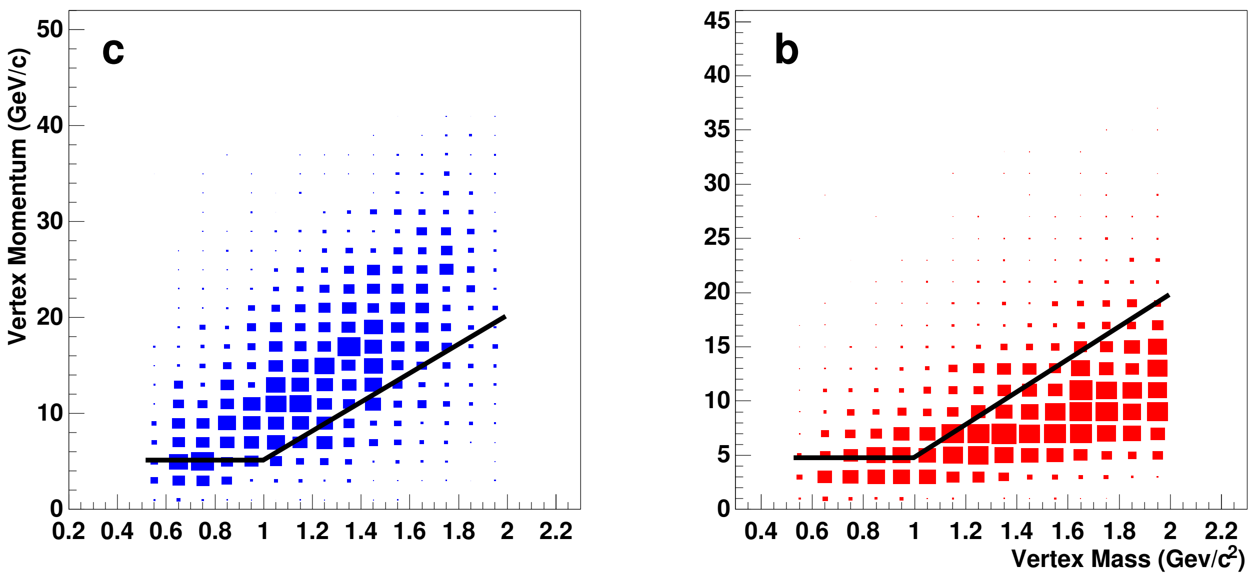

Figure 9: Vertex momentum vs vertex mass for $b\bar{b}$ and $c\bar{c}$ events.

4 The SLD CRID

Identification of charged tracks in the SLD is accomplished with the Cherenkov Ring Imaging Detector (CRID) [5]. By measuring the emission angles of individual Cherenkov photons radiated by charged particles traversing liquid (C_6F_{14}) and gaseous (C_5F_{12}+N_2) radiators, the CRID is designed to provide efficient charged $\pi/K/$p identification over most of the momentum range in e^+e^- annihilations at the Z^0, 0.3–46 GeV/c, as well as lepton identification for $p < 8$ GeV/c. Tremendous progress has been made in the last few years in understanding the barrel CRID, which covers the polar angle range $|\cos\theta| \leq$0.68, culminating in reaching design resolution in local Cherenkov angle resolution. An exhaustive alignment procedure has resulted in excellent system resolution in the liquid (gas) Cherenkov angle of 16(4.5) mrad. The average number of detected photons per full liquid (gas) ring in μ-pair events is 16.1 (10.0) [6]. For hadronic events, cuts were optimized to reduce backgrounds from spurious hits, especially those due to cross-talk from saturating hits, resulting in a reduction to 12.8 (9.2) hits.

Charged hadrons are identified using a likelihood technique [7] that considers random backgrounds as well as those from other tracks in the event, and accounts smoothly for Cherenkov thresholds. The performance of the CRID must be optimized for each type of analysis. In our hadron fractions analysis we quantify the performance in terms of a momentum-dependent matrix of efficiencies for identifying a track from a true i-hadron as a j-hadron, $i, j = \pi, K$, p, which is shown in fig. 10. Each efficiency is shown as a pair of smooth curves representing the $\pm 1\sigma$ uncertainty on the efficiency. The functional forms of these curves were determined from a detailed detector simulation, and their parameters and uncertainties were determined from the data, using samples of tagged K_s, Λ^0 and τ decays. Pions are identified with high efficiency from 0.3 to 35 GeV/c. Kaons and protons are also identified over most of this range, although they cannot be distinguished in the 7–10 GeV/c range. Kaons and protons are both separated from pions over the entire range, which is sufficient for many applications. Misidentification rates are low, typically below about 2%, with peaks up to 6%.

5 Improvements in Detector Performance

SLD's present performance in tracking and vertexing, hadron identification, and lepton identification is already very impressive. We are continuing to improve this performance in ways that will significantly impact future physics measurements.

Tracking coverage and tracking quality have been improved by adding information from VXD3 at the pattern recognition stage. Since the vertex detector can fully determine track position and angle, it is a powerful pattern recognition device. With this new approach, tracking solid angle coverage has been extended to 85% with full efficiency, and to 90% for most tracks. Impact parameter resolution continues to improve with better CCD alignment techniques and track fitting strategies. We have recently identified that the performance of our track fitting algorithms is less than optimal for reconstruction in both r-ϕ and r-z planes, and devised corrections that will boost the r-z resolution to be comparable to that in

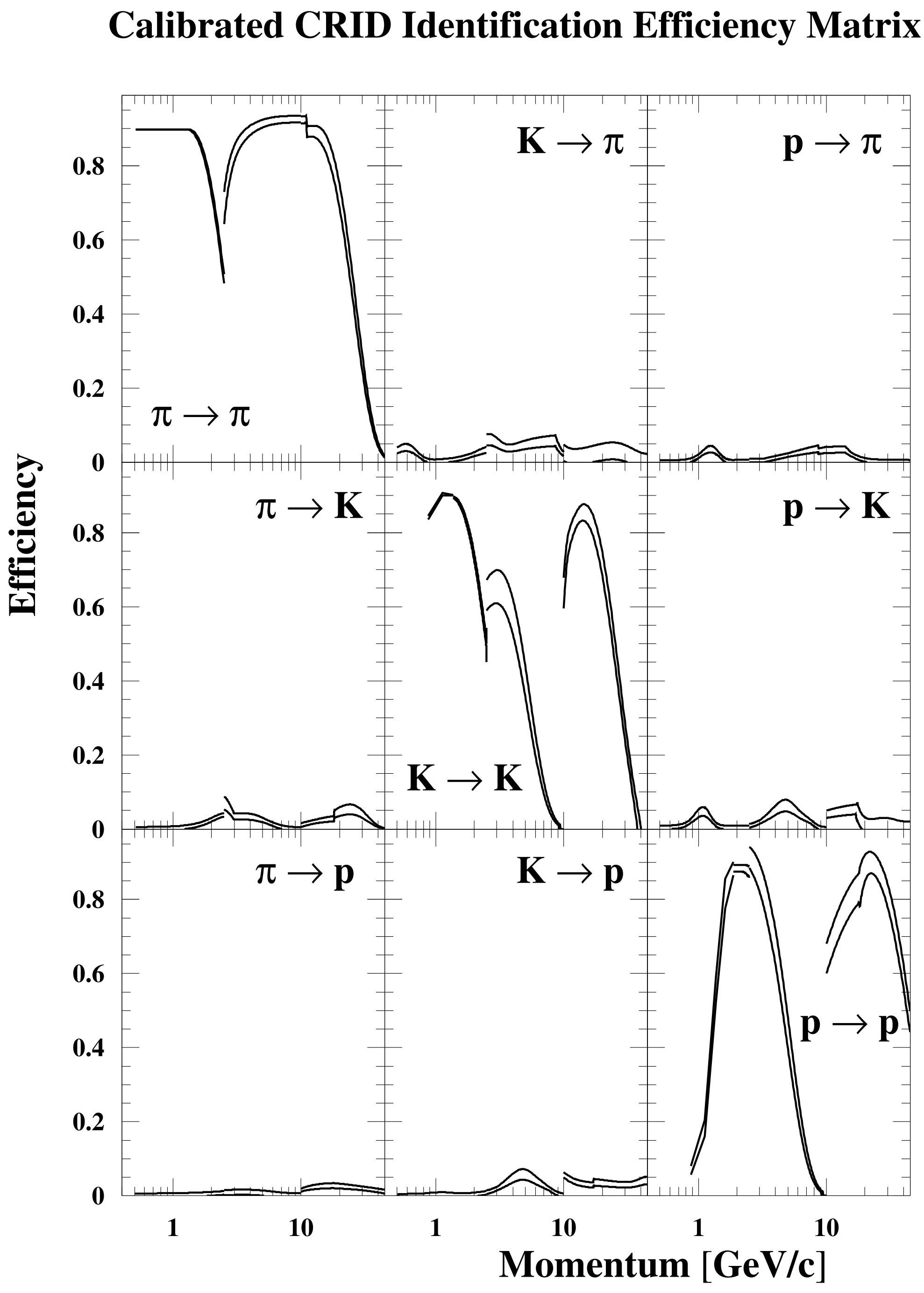

Figure 10: Matrix of identification efficiencies for true $\pi^{\pm}$, $K^{\pm}$, and p/$\bar{\text{p}}$ to be identified as each of these three particle types as a function of track momentum.

r-ϕ. Decay length resolutions will improve by about 20% compared to present performance.

It has at last been demonstrated is that it is possible to use the End Cap Drift Chamber to determine the charge of high-momentum muon pairs. Prior to the 1996 run an "EndCap Muon Trigger" was installed to allow for selection of μ-pair candidates. This extended the polar angle coverage from $|\cos\theta| = 0.7$ to 0.9 for μ-pair selection. Vertex detector information is used in these events to determine track directions, assuming that the tracks originated at the IP. Each of the two tracks is assumed to have momentum of $\sqrt{s}/2$. Using this technique to extend the polar angle coverage, clear charge separation is possible. The resulting statistical gain in the measurement of A_μ is expected to be approximately 20% .

There is work underway to extend the solid-angle coverage for muon identification. To identify muons, the traditional procedure has been to use multi-layer WIC information in the barrel region ($|\cos\theta| < 0.70$). Unfortunately, the ID efficiency falls rapidly near the edges of this acceptance ($0.60 < |\cos\theta| < 0.70$). There are several approaches that can be taken to improve muon coverage. First, in the "45 degree region" where the ID efficiency falls off rapidly, information from the WIC 45 deg chambers might be utilized. Alternately, a combination of CDC track information and fewer layers of barrel WIC information could be used. A third technique, which has shown promising initial results, uses a neural net algorithm to combine WIC and LAC information. For tracks above 7 GeV/c, MC studies indicate that the muon ID efficiency and purity for this approach is $\sim$54% and $\sim$72%, respectively, in the polar angle region $0.60 < |\cos\theta| < 0.80$. Using EndCap LAC and EndCap WIC information, it seems possible to extend this technique to $|\cos\theta| < 0.90$ with efficiencies and purities that are similar to the central region.

Part IV
The Physics Program

6 Electroweak Physics

6.1 Introduction

A polarized e^+e^- collider operating at the Z-peak is an ideal device to study the neutral current couplings of leptons and quarks. The fermionic couplings of the Z can be characterized by the following Lagrangian,

$$\begin{aligned} \mathcal{L} &= \frac{1}{2}\left(\frac{G_F M_Z^2}{\sqrt{2}}\right)^{1/2} \overline{\Psi}_f \gamma_\mu \left(v_f - a_f \gamma_5\right) \Psi_f Z^\mu \qquad (1) \\ &= \frac{1}{2}\left(\frac{G_F M_Z^2}{\sqrt{2}}\right)^{1/2} \overline{\Psi}_f \gamma_\mu \left[g_L^f \left(1-\gamma_5\right) + g_R^f \left(1+\gamma_5\right)\right] \Psi_f Z^\mu \end{aligned}$$

where v_f,a_f are vector and axial vector coupling constants and g_L^f, g_R^f are equivalent left- and right-handed coupling constants. The couplings v_f and a_f incorporate electroweak radiative corrections and can be expressed as follows,

$$v_f = \sqrt{\rho_f}\left(2I_3^f - 4Q_f \sin^2\theta_f\right) \qquad (2)$$

$$a_f = \sqrt{\rho_f}\left(2I_3^f\right), \qquad (3)$$

where I_{3L}^f is the third component of weak isospin for the left-handed fermion f, Q_f is the charge of the fermion, ρ_f is an effective strength for the $Zf\bar{f}$ coupling, and θ_W^f is an effective weak mixing angle for the $Zf\bar{f}$ coupling. The effective weak mixing angle incorporates universal (flavor-indepdendent) vacuum polarization corrections from the Z propagator and flavor-dependent vertex corrections. The Minimal Electroweak Standard Model (MSM) predicts that the flavor-dependent corrections are quite small (except perhaps for the b-quark current) and that a single effective mixing angle can describe all fermion currents. It is conventional to define the effective weak mixing angle as the one that applies to the Ze^+e^- vertex, $\sin^2\theta_W^{\text{eff}} = \sin^2\theta_W^e$.

Measurements of partial decay widths of the Z-boson are proportional to the sum of the squares of v_f and a_f,

$$\Gamma_{Z\to f\bar{f}} = \frac{G_F M_Z^3}{24\pi\sqrt{2}}\left(v_f^2 + a_f^2\right) \qquad (4)$$

The LEP experiments have measured the partial widths of Z decays into each of the lepton flavors, b-quarks, c-quarks, and all hadrons. The SLD Collaboration has measured the partial widths for b-quark and c-quark final states.

Measurements of the various Z-pole asymmetries determine the quantities A_f which are functions of the ratios v_f/a_f,

$$A_f \equiv \frac{2v_f a_f}{v_f^2 + a_f^2} = \frac{2\,(v_f/a_f)}{(v_f/a_f)^2 + 1}. \tag{5}$$

Due to a numerical accident, the leptonic ratios v_ℓ/a_ℓ are much smaller than the quark ratios. Since electroweak radiative corrections modify each v_f/a_f ratio by similar amounts, the fractional effect of the corrections is much larger for the leptonic ratios.

The quantities A_e, A_μ, A_τ, A_b, A_c, and A_s have been determined by a series of measurements performed at LEP and SLC. The LEP measurements fall into two categories: forward-backward asymmetry measurements and final-state τ-polarization measurements. The forward-backward asymmetry measurements, performed with unpolarized beams, determine the product of A_e and A_f,

$$A_{FB}^f \equiv \frac{\sigma_F^f - \sigma_B^f}{\sigma_F^f + \sigma_B^f} = \frac{3}{4} A_e A_f, \tag{6}$$

where σ_F^f and σ_B^f are the cross sections for the process $e^+e^- \to Z \to f\bar{f}$ integrated over the forward (f in the electron direction) and backward (f in the positron direction) hemispheres, respectively. The τ-polarization measurements determine A_τ from the average final state polarization and A_e from the angular dependence of the τ polarization.

The SLD measurements are performed with a polarized electron beam and also fall into two categories: the left-right asymmetry measurement and left-right forward-backward asymmetry measurements. The left-right asymmetry is defined as,

$$A_{LR} = \frac{\sigma^f(-|\mathcal{P}_e|) - \sigma^f(+|\mathcal{P}_e|)}{\sigma^f(-|\mathcal{P}_e|) + \sigma^f(+|\mathcal{P}_e|)} = |\mathcal{P}_e| A_e, \tag{7}$$

where $\mathcal{P}_e$ is the average longitudinal polarization of the electron beam in a right-handed helicity basis. Note that for $f \neq e$, the cross section is entirely s-channel and the left-right asymmetry is independent of final state couplings and radiative effects. The final state couplings can be studied independently of the initial-state coupling by forming the left-right forward-backward asymmetries which are defined as,

$$\tilde{A}_{FB}^f = \frac{\sigma_F^f(-|\mathcal{P}_e|) - \sigma_F^f(+|\mathcal{P}_e|) - \sigma_B^f(-|\mathcal{P}_e|) + \sigma_B^f(+|\mathcal{P}_e|)}{\sigma_F^f(-|\mathcal{P}_e|) + \sigma_F^f(+|\mathcal{P}_e|) + \sigma_B^f(-|\mathcal{P}_e|) + \sigma_B^f(+|\mathcal{P}_e|)} = \frac{3}{4}|\mathcal{P}_e| A_f. \tag{8}$$

The SLD Collaboration has performed measurements of the left-right forward-backward asymmetries for leptonic, b-quark, c-quark, and s-quark final states.

The measurements of A_e, A_μ, and A_τ are quite sensitive to vacuum polarization corrections and are used to determine $\sin^2\theta_W^{\rm eff}$. The measurements of A_b, A_c, and A_s are relatively insensitive to vacuum polarization corrections and are used to search for vertex corrections beyond those predicted by the MSM.

6.2 SLD Measurements of $\sin^2\theta_W^{\rm eff}$

The SLD Collaboration has determined the parameter $\sin^2\theta_W^{\rm eff}$ from measurements of the left-right asymmetry [8], the left-right forward-backward asymmetries of leptonic final states [9], and the polarized, forward-backward hadronic jet charge asymmetry [10]. The measurements of A_{LR} are the most precise and dominate the average.

The left-right asymmetry is measured by counting hadronic and (with low efficiency) $\tau^+\tau^-$ final states produced in e^+e^- collisions near the Z-pole energy for each of the two longitudinal polarization states of the electron beam. The raw asymmetry formed from these numbers (approximately 0.12) is corrected for very small residual effects (approximately 0.0002) arising from unsubtracted backround and residual asymmetries in beam current, energy, and polarization. The asymmetry is then divided by the beam polarization (0.73-0.77 depending upon electron source photocathode) and is corrected for residual effects (approximately 0.003) arising from pure photon exchange and Z-photon interference to extract A_e (approximately 0.15). The measurement requires knowledge of the absolute beam polarization, but does not require knowledge of the absolute luminosity, detector acceptance, or efficiency. The properties of the measured asymmetry (A_{LR}) are contrasted with those of the other Z pole asymmetries in Table 2. Assuming a beam polarization of 80%, the measurement of A_{LR} has 100-300 times more statistical power and is more precise systematically than measurements of the other observables.

Table 2: Comparison of various Z-pole observables.

	A_{LR}	A_{FB}^{ℓ}	A_{FB}^{b}	P_τ
MSM:				
Asymmetry	0.12	0.02	0.11	0.15
Sensitivity: $\partial A/\partial\sin^2\theta_W^{\rm eff}$	6.3	1.2	5.6	7.9
Events:				
Usable fraction of Z decays	0.96	0.12	0.19	0.04
Efficiency-Acceptance	0.90	0.7-0.8	0.10	0.30
Relative Z sample for equal statistical precision	1	250	100	320
Systematics:				
Beam Polarization	yes	no	no	no
Efficiency-Acceptance	no	yes	yes	yes
Backgrounds	no	no	yes	yes
Decay Modelling	no	no	yes	no
B Mixing	no	no	yes	no
Final State Radiation	no	yes	yes	yes
E-W Interference Correction	2%	100%	5%	2%

A summary of six A_{LR} measurements performed from 1992 to the end of the 1998 run is presented in Table 3. The 1997 and 1998 results are preliminary and are based on approximately 300K Z events logged before late May 1998. The systematic uncertainties are dominated by the polarization scale uncertainties discussed in Section 2. The six measured values of $\sin^2\theta_W^{\rm eff}$ are presented graphically in Fig. 11. The average value and its uncertainty are shown as a band and are compared with the average of thirty measurements performed by the LEP Collaborations [11]. Note the the SLD result differs from the LEP average of $\sin^2\theta_W^{\rm eff} = 0.23187 \pm 0.00024$ by approximately 2.2 standard deviations. The SLD and LEP results are plotted versus technique Fig. 12. Note that most of the discrepancy is due to a 2.5 standard deviation difference between the A_{LR} measurement and the b-quark forward-backward asymmetry measurements. This discrepancy may be due to unknown systematic effects that affect one or both of the measurements. A second possibility is that the parameter $\sin^2\theta_b$ defined in equation 2 differs from $\sin^2\theta_e$ due to new physical processes that affect the $Zb\bar{b}$ vertex. This latter possibility is discussed in Section 6.3.2.

Table 3: 1992-1998 SLD Measurements of A_{LR}.

Year	A_e	$\sin^2\theta_W^{\rm eff}$
1992	$0.100 \pm 0.044 \pm 0.004$	$0.2378 \pm 0.0056 \pm 0.0005$
1993	$0.1656 \pm 0.0071 \pm 0.0028$	$0.2292 \pm 0.0009 \pm 0.0004$
1994/5	$0.1512 \pm 0.0042 \pm 0.0011$	$0.23100 \pm 0.00054 \pm 0.00014$
1996	$0.1570 \pm 0.0057 \pm 0.0011$	$0.23025 \pm 0.00073 \pm 0.00014$
1997	$0.1475 \pm 0.0042 \pm 0.0016$	$0.23146 \pm 0.00054 \pm 0.00020$
1998	$0.1487 \pm 0.0031 \pm 0.0017$	$0.23130 \pm 0.00039 \pm 0.00022$
Total	0.1510 ± 0.0025	0.23101 ± 0.00031

6.2.1 Interpretation of $\sin^2\theta_W^{\rm eff}$ Measurements

As was mentioned in Section 6.1, the parameter $\sin^2\theta_W^{\rm eff}$ is quite sensitive to gauge boson vacuum polarization effects. It has been shown [12] that since all electroweak observables have been measured at two scales ($q^2 = 0,\ M_Z^2$), the vacuum polarization effects can be characterized by three parameters. A number of three-parameter schemes have been proposed. This document makes use of the S, T, U scheme of Peskin and Takeuchi.

The S parameter is weak isospin symmetric and characterizes the size of the sector that contributes to Π_{33}. It has a logarithmic dependence on m_t and m_H. The T parameter characterizes the degree of breaking of the custodial SU(2) symmetry that ensures the unity of the ρ parameter. It has an approximately quadratic dependence upon m_t and a logarithmic dependence upon m_H. In the MSM and many of its extensions, the U parameter is associated with somewhat smaller corrections than are S and T. It has a logarithmic dependence upon m_t and is independent of m_H. The effective Lagrangian for neutral current processes depends upon S and T only. The charged current effective Lagrangian depends upon S, T, and U. Since most of the electroweak observables that have been measured concern neutral current processes, and since U is associated with small effects in well-studied theories, it is customary to assume that U is zero.

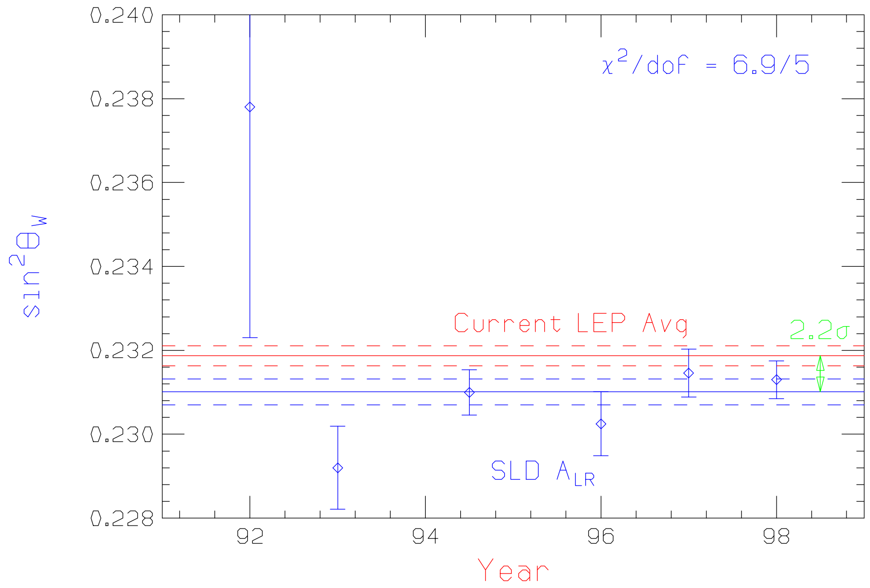

Figure 11: The five values of $\sin^2\theta_W^{\rm eff}$ extracted from measurements of A_{LR} are plotted as a function of time. The bands show the SLD and LEP average values of $\sin^2\theta_W^{\rm eff}$.

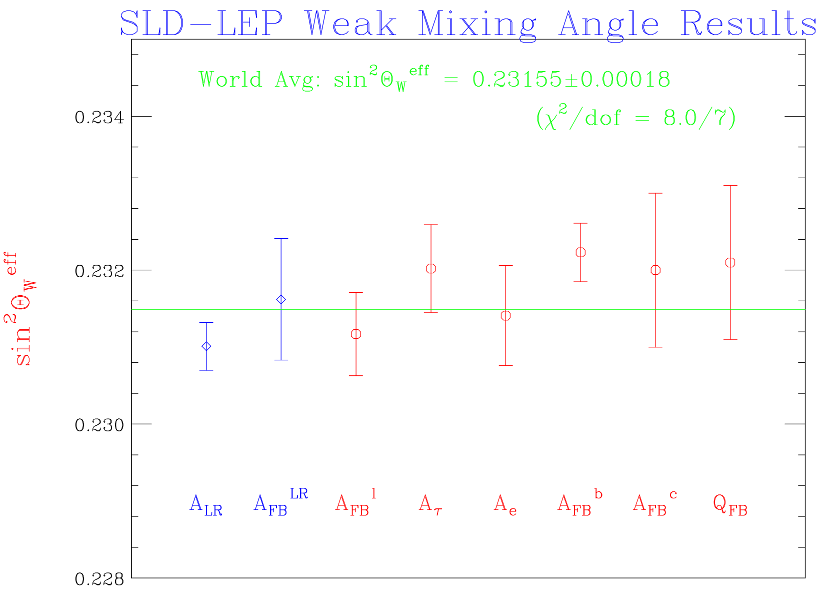

Figure 12: A comparison of $\sin^2\theta_W^{\rm eff}$ measurements by technique. The average of the SLD measurements (shown as diamonds) is $\sin^2\theta_W^{\rm eff} = 0.23110 \pm 0.00029$. The average of the LEP measurements (shown as circles) is $\sin^2\theta_W^{\rm eff} = 0.23187 \pm 0.00024$. The world average is $\sin^2\theta_W^{\rm eff} = 0.23155 \pm 0.00018$.

The SLD and LEP measurements of $\sin^2\theta_W^{\rm eff}$ determine the 68% confidence regions in S-T space shown in Figure 13. The 68% confidence regions determined by the world average values of the W-boson mass, the width of the Z-boson, and the ratio of charged- and neutral-current neutrino cross sections are also shown in the figure. A fit to all of the world's electroweak data determines the 68% elliptical confidence region also shown in the figure. The region of S-T space predicted by the Minimal Standard Model is shown as the banana-shaped region. The right-hand edge of the region corresponds to the MSM prediction for $m_H = 88$ GeV and $m_t = 173.9 \pm 5.2$ GeV. Continuously increasing the Higgs boson mass to 1 TeV, sweeps out the bounded area. It is clear that the global fit is consistent with the MSM. Note, however, that the SLD $\sin^2\theta_W^{\rm eff}$ measurement favors a light Higgs boson and that in the absence of the LEP $\sin^2\theta_W^{\rm eff}$ measurements, the measured bands would overlap in the region of negative S. The predictions of the Minimal Supersymmetric Standard Model (MSSM) are shown [13] on the plot as a series of small circular points. Each point consists of a separate choice for the five parameters of the MSSM. The SLD $\sin^2\theta_W^{\rm eff}$ measurement is quite consistent with the MSSM region whereas the LEP measurement deviates by approximately two sigma from it.

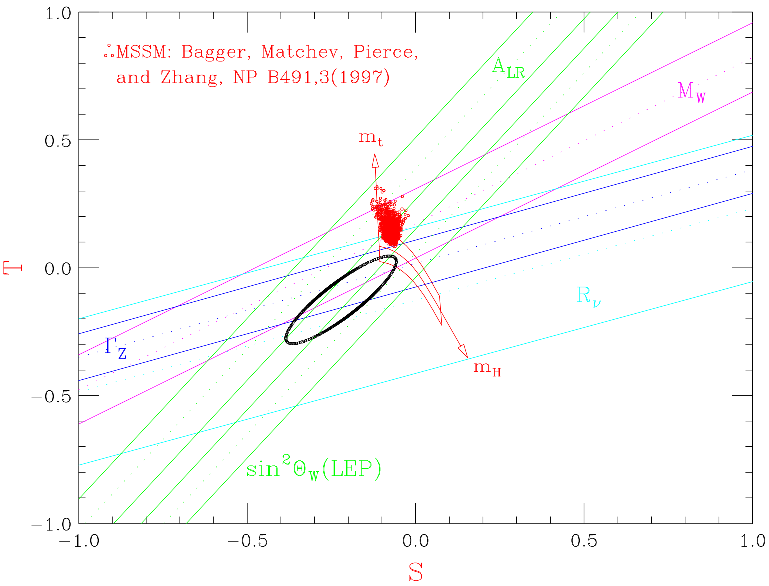

Figure 13: The 68% confidence regions in S-T space determined by: the measured value of A_{LR}, the LEP measurement of $\sin^2\theta_W^{\rm eff}$, the world average values of the W-boson mass, the width of the Z-boson, and the ratio of charged- and neutral-current neutrino cross sections. A fit to all of the world's electroweak data determines the 68% elliptical confidence region. The region of S-T space predicted by the Minimal Standard Model is shown as the banana-shaped region. The predictions of the Minimal Supersymmetric Standard Model (MSSM) are shown [13] as a series of small circular points.

The SLD $\sin^2\theta_W^{\rm eff}$ measurement is compared with the predictions of the Minimal Standard

Model in Figure 14. The MSM prediction [14] for $m_t = 173.9(\pm 5.2)$ GeV is shown as the solid (central m_t value) and dashed (± 1 sigma) curves as a function of m_H. The measurement is plotted as a box at the most probable mass value. The dashed-dotted lines show the 68% confidence region in m_H-space that is determined by the SLD data. The average LEP measurement is plotted as an X in the same way and the 68% confidence region in m_H-space is also shown by the dashed-dotted lines. It is clear that both measurements are consistent with the MSM. The SLD measurement prefers light Higgs masses and the LEP result favors heavier values.

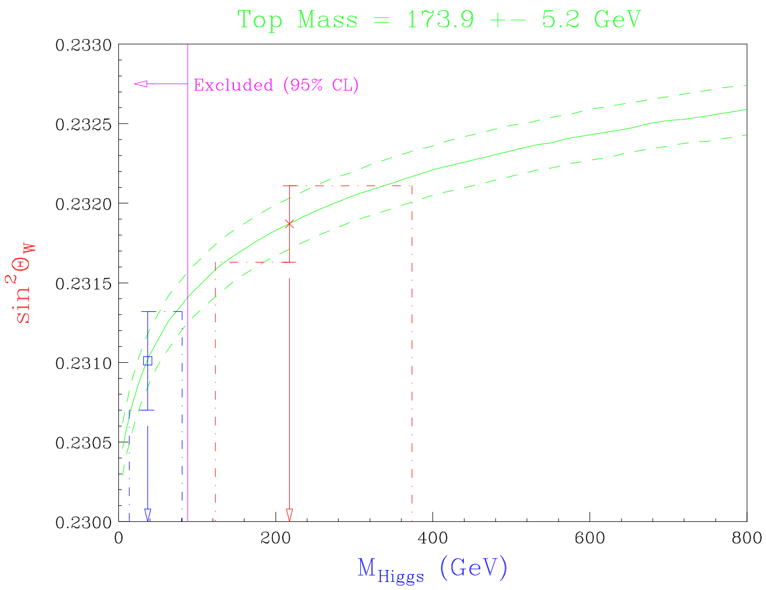

Figure 14: The MSM prediction for $\sin^2\theta_W^{\rm eff}$ (from ZFITTER 5.10) is plotted versus m_H for $m_t = 173.9 \pm 5.2$ GeV. The SLD measurement is shown as a box and the LEP measurement is shown as an X. The dashed-dotted lines show the 68% confidence regions in m_H-space determined by the $\sin^2\theta_W^{\rm eff}$ measurements.

6.2.2 Future of the A_{LR} Measurement

The 2.2 σ difference between the LEP and SLD results is not statistically significant but has physical consequence. Confirmation of the SLD central value of $\sin^2\theta_W^{\rm eff}$ with smaller errors would provide the first evidence that the MSM is incomplete or incorrect. It would strengthen the case that nature might be supersymmetric. It would also support the possibility that S is negative which would eliminate many of the currently possible theoretical scenarios.

The total error on $\sin^2\theta_W^{\rm eff}$ expected from an extended SLD run is shown in Figure 15. Extending the 1997-1998 data set to one million Z-events would permit the measurement of $\sin^2\theta_W^{\rm eff}$ with a precision of ± 0.00018 which is smaller than the current result (including the preliminary 1997/8 data) by a factor of nearly two. If the central value of such a measurement did not change, it would exclude the MSM at the 95% level.

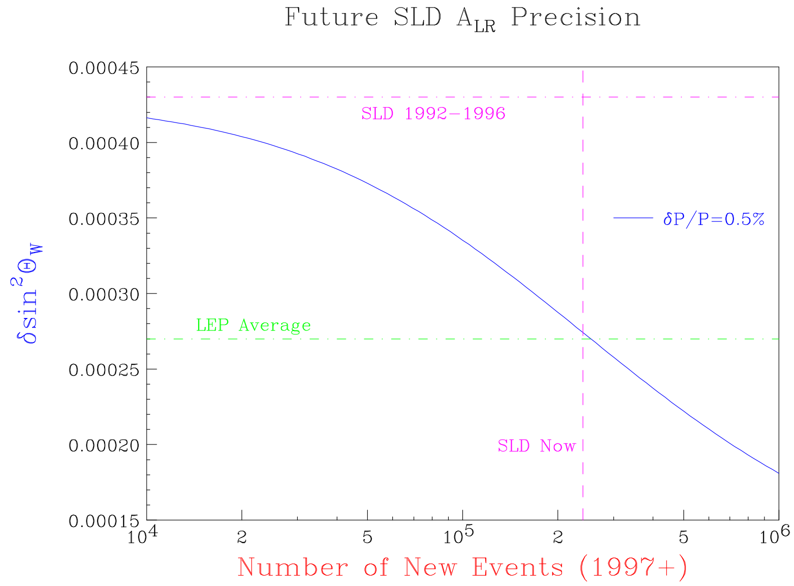

Figure 15: The total uncertainty on $\sin^2\theta_W^{\rm eff}$ as a function of the number of Z events collected since the beginning of the 1997/8 run.

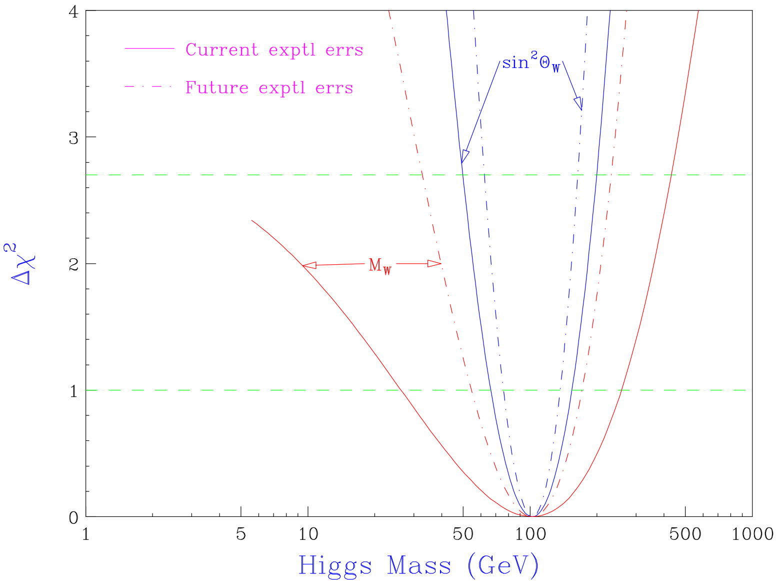

Figure 16: The χ^2 of 0-constraint fits to $\sin^2\theta_W^{\rm eff}$ and M_W determinations are plotted versus m_H for measurements with the current world average uncertainties (± 0.00019 for $\sin^2\theta_W^{\rm eff}$ and ± 60 MeV for M_W) as solid curves and as dashed-dotted curves for future world average uncertainties (± 0.00014 for $\sin^2\theta_W^{\rm eff}$ and ± 30 MeV for M_W).

The reader should note that the $\sin^2\theta_W^{\rm eff}$ measurements constitute the most precisely determined high-energy electroweak parameter after the Z mass. The combined SLD/LEP result determines the smallest region on the S-T plot. The m_H sensitivity of the current world average $\sin^2\theta_W^{\rm eff}$ measurement is compared with that of the world average M_W measurement in Fig. 16. The change in the χ^2 of 0-constraint fits to $\sin^2\theta_W^{\rm eff}$ and M_W determinations are plotted versus m_H for measurements with the current world average uncertainties (±0.00019 for $\sin^2\theta_W^{\rm eff}$ and ±60 MeV for M_W) as solid curves. To simplify the comparison, the central values of the measurements have been taken to correspond to $m_H = 100$ GeV. The same information is plotted for *ultimate* precisions, ±0.00014 for $\sin^2\theta_W^{\rm eff}$ and ±30 MeV for M_W, as dashed-dotted curves. Note that the Higgs mass sensitivity of the current world average $\sin^2\theta_W^{\rm eff}$ measurement is already better than future M_W measurements at LEP and the Tevatron will provide. The proposed SLD measurement would produce a determination of $\log(m_H)$ that would be a factor of two better than the future M_W measurements will provide. It is clear that performing the best possible measurement of $\sin^2\theta_W^{\rm eff}$ and 'Getting it Right' will be crucial and longlasting contributions to electroweak physics.

6.3 Electroweak Measurements with Heavy Flavor Final States

As was mentioned in section 6.1, the effective couplings v_f and a_f are also affected by electroweak vertex corrections. Within the context of the MSM, the vertex corrections are generally small and uninteresting [the left-handed b-quark coupling $g_L^b \equiv (v_b + a_b)/2$ does receive a measurably large contribution from the heavy t-quark]. However, many extensions to the MSM could produce larger, flavor-dependent effects. Of particular interest are b-quark final states. In many theories, the relatively heavy b-quark current receives large vertex corrections. Experimentally, samples of high purity can be efficiently isolated from other hadronic final states (see Section 3). The SLD Collaboration has used its superior vertexing to measure the ratio of the $Z \to b\bar{b}$ and $Z \to$ hadrons widths, $R_b \equiv \Gamma_{b\bar{b}}/\Gamma_{had}$, and the asymmetry A_b. SLD's three-dimensional vertexing and vertex mass tag also permit the efficient tagging of relatively pure c-quark final states and enable the measurement of R_c and A_c.

6.3.1 The R_b and R_c Measurements

The quantities R_b and R_c are essentially independent of QCD corrections and vacuum polarization effects (which cancel in the ratios of partial widths). They are measured using the so-called *double-tag method* in which heavy quark tagging procedures are applied independently to each thrust hemisphere of all hadronic Z events. One then measures the rates of tagged-hemispheres (b_s,c_s), double-tag events (b_d,c_d), and mixed-tag events (m). These rates are related to R_b and R_c by the following equations,

$$b_s = 2\left[\varepsilon_b R_b + \varepsilon_c R_c + \varepsilon_{uds}\left(1 - R_b - R_c\right)\right] \tag{9}$$

$$b_d = \varepsilon_b^d R_b + \varepsilon_c^d R_c + \varepsilon_{uds}^d\left(1 - R_b - R_c\right) \tag{10}$$

$$c_s = 2\left[\eta_b R_b + \eta_c R_c + \eta_{uds}\left(1 - R_b - R_c\right)\right] \tag{11}$$

$$c_d = \eta_b^d R_b + \eta_c^d R_c + \eta_{uds}^d\left(1 - R_b - R_c\right) \tag{12}$$

$$m = 2\left[\varepsilon_b \eta_b R_b + \varepsilon_c \eta_c R_c + \varepsilon_{uds} \eta_{uds} \left(1 - R_b - R_c\right)\right], \tag{13}$$

where: ε_x is the probability of a quark-jet of flavor x ($x = b, c, s, d, u$) to satisfy the b-tag, ε_x^d is the probability that both quark-jets of flavor x to satisfy the b-tag, η_x is the probability of a quark-jet of flavor x to satisfy the c-tag, and η_x^d is the probability that both quark-jets of flavor x to satisfy the c-tag. The double-tag probabilities are related to the single-tag probabilities by the following expressions,

$$\varepsilon_x^d = \varepsilon_x^2 + \lambda_x \tag{14}$$

$$\eta_x^d = \eta_x^2 + \lambda'_x, \tag{15}$$

where the terms λ_x and λ'_x account for inter-hemisphere correlations (since ε_{uds} and η_{uds} are small, the correlation terms λ_{uds} and λ'_{uds} can be assumed to be zero).

The R_b measurement is performed by solving equations 9 and 10. The quantity R_c is set to its MSM value and the quantities ε_c, ε_{uds}, λ_b are calculated from a Monte Carlo simulation. The equations are then solved simultaneously for R_b and ε_b. This technique avoids the large systematic uncertainties associated with the calculation of ε_b that limit single-tag analyses.

The most recent SLD measurement of R_b is shown in Figure 17 along with six measurements from the LEP Collaborations. The measurement is based upon the 150,000 Z sample logged with VXD2 and 250,000 Z events logged in 1996-1998 with VXD3. Note that its precision is comparable to individual LEP measurements and the central value agrees well with the MSM. Most of the recent LEP measurements heave now adopted improved b-tags using vertex mass information and yield results which agree well with the MSM. Some of the previous generation of LEP measurements with less pure tagging techniques measured values which were significantly above the MSM expectation. One possible interpretation is that the level of $udsc$ background contamination was systematically underestimated by the physics/detector simulations.

The R_c measurement is performed by solving equations 9-13. The Monte Carlo simulation is used to calculate the quantities ε_c, ε_{uds}, λ_b, η_{uds}, λ'_b, and λ'_c. The five-equation set is then solved for R_c, η_c, η_b, R_b, and ε_b.

The most recent SLD measurement of R_c is shown in Figure 18 along with 10 measurements from the LEP Collaborations. The measurement is based upon the 150,000 Z sample logged with VXD2 and the 150,000 Z events logged in 1996 and 1997 with VXD3. Note that it compares well with individual LEP measurements. The total error is expected to decrease from ± 0.011 to ± 0.007 when the 1998 data are included in the analysis.

6.3.2 The A_b and A_c Measurements

The asymmetry parameters A_b and A_c are extracted from fits to the polarized angular distributions of tagged $b\bar{b}$ and $c\bar{c}$ events. To perform these analyses, it is not only necessary to tag the heavy quark final states, but one must also identify which hemisphere contains the quark and which contains the antiquark. Several different techniques are used for each measurement.

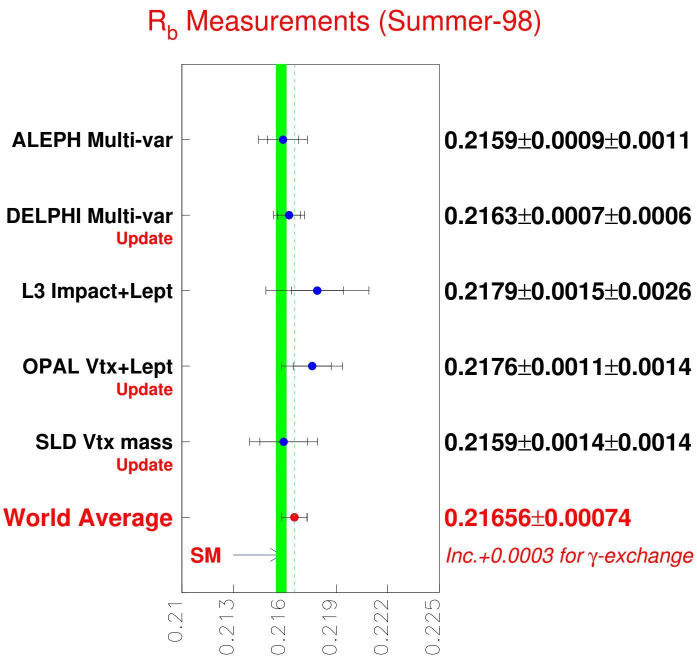

Figure 17: A summary of all measurements of R_b.

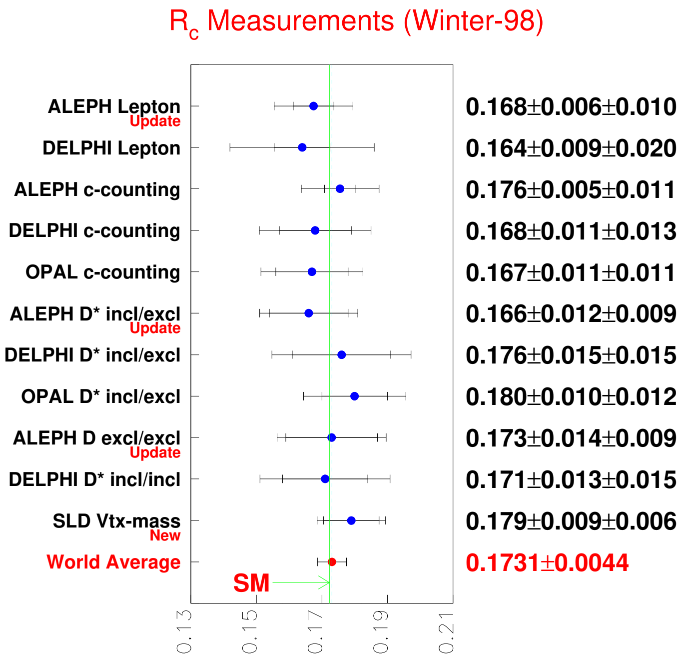

Figure 18: A summary of all measurements of R_c.

The b-quark asymmetry parameter is measured by three different techniques. The first technique uses mass-tagging to identify the final states and jet-charge techniques to sign-identify the hemispheres. The second technique uses the same tagging technique but uses the CRID to count $K^{\pm}$ tracks in each hemisphere. The charged kaons are produced in the cascade decay $b \to c \to s$ and have a correct flavor-sign probability (~ 0.7) comparable to the jet-charge technique. The third technique makes use of large momentum, large P_T leptons (electrons and muons) both to tag the final state and to sign identify the hemispheres. The results of these measurements are shown in Figure 19. The combined result is 1.9 σ smaller than the MSM expectation ($A_b = 0.935$). The LEP Collaborations measure the unpolarized b-quark forward-backward asymmetry A^b_{FB} which is proportional to the product of A_e and A_b. Taking A_e from the average of all leptonic measurements A_ℓ, the parameter A_b is extracted from the A^b_{FB} measurements. The LEP A_b average is approximately 2.3 σ smaller than the MSM value. The combination of the LEP and SLD results, $A_b = 0.880 \pm 0.019$, is about 2.9 standard deviations less than the MSM value.

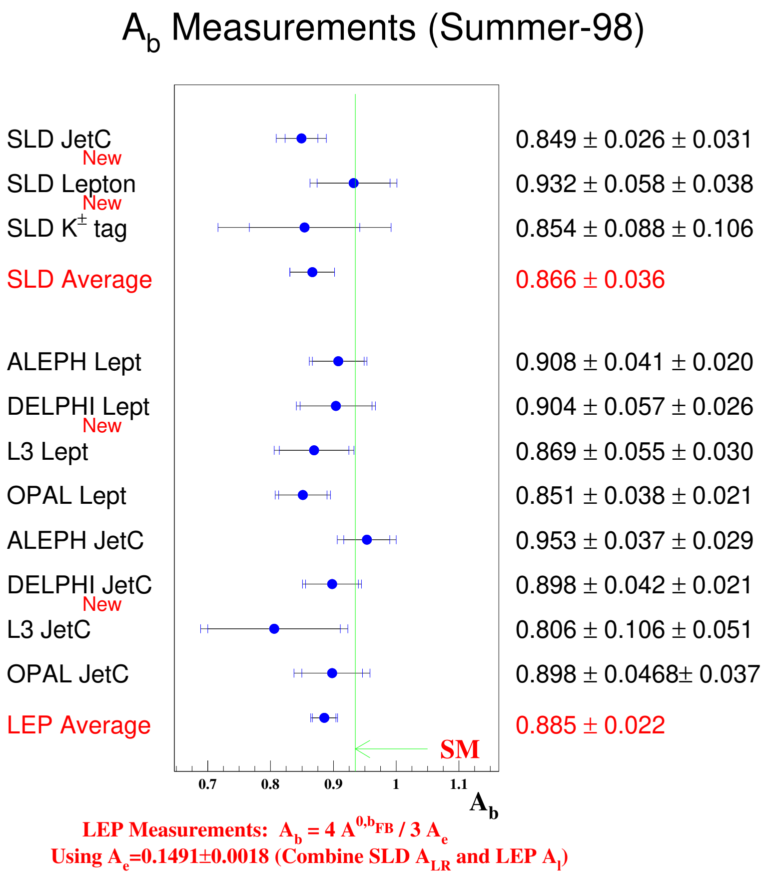

Figure 19: A summary of all determinations of A_b.

The c-quark asymmetry parameter is measured by four different techniques. The first technique uses mass-tagging to identify the final states and the charge of a reconstructed secondary vertex to sign-identify the hemispheres. The second technique uses the same tagging technique but uses the CRID to count $K^{\pm}$ tracks in each hemisphere (from the decay $c \to s$). The third technique makes use of moderate momentum, moderate P_T leptons (electrons and muons) to both tag the final state and to sign identify the hemispheres. The final technique uses reconstructed D and D^* mesons to perform both tasks. The results of these measurements are shown in Figure 20. The combined result is consistent with the MSM expectation. The LEP Collaborations measure the unpolarized c-quark forward-backward asymmetry A^c_{FB} which is proportional to the product of A_e and A_c. Taking A_e from the average of all leptonic measurements A_ℓ, the parameter A_c is extracted from the A^c_{FB} measurements. Note that, with only a partial data sample, the preliminary direct SLD measurement has a precision equal to the current LEP average.

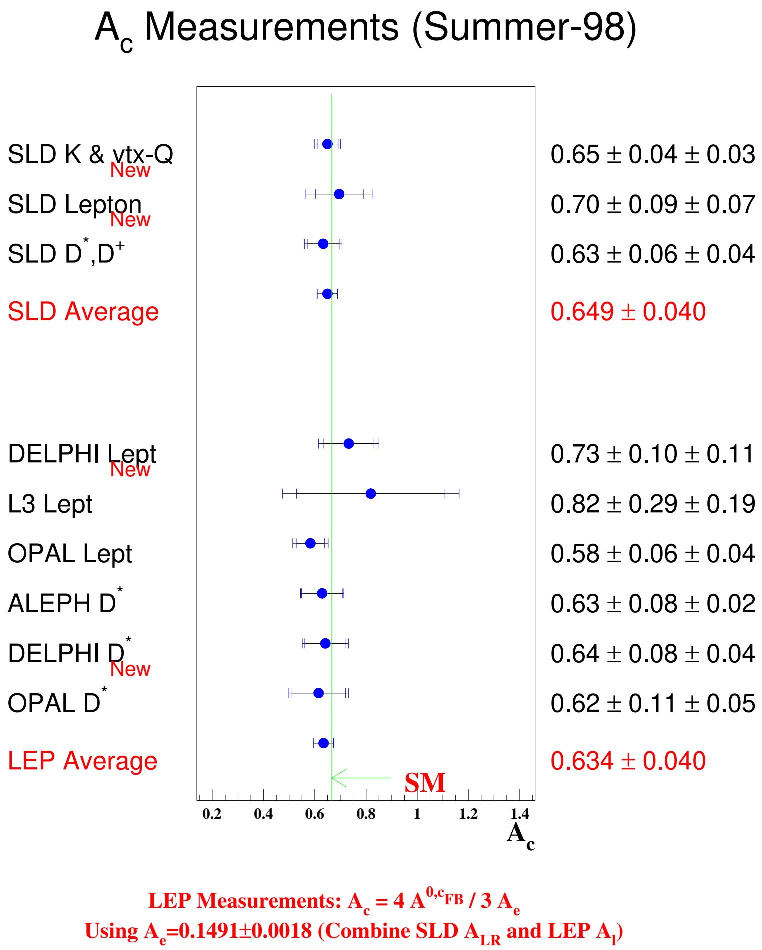

Figure 20: A summary of all determinations of A_b.

6.3.3 Interpretation of b-quark Measurements

It is convenient to parameterize the b-quark couplings into an STU-like formalism that represents deviations from the Minimal Standard Model. In the $\xi_b\zeta_b$ scheme of Takeuchi, Grant, and Rosner [15], the parameters $\delta s^2, \delta g_L^b, \delta g_R^b$ represent deviations of $\sin^2\theta_W^{\rm eff}, g_L^b, g_R^b$ from their MSM values at a conveniently chosen reference point ($m_t = 175$ GeV, $m_H = 300$ GeV),

$$\sin^2\theta_W^{\rm eff} = \left[\sin^2\theta_W^{\rm eff}\right]_{ref} + \delta s^2 \tag{16}$$

$$g_L^b = \left[g_L^b\right]_{ref} + \frac{1}{3}\delta s^2 + \delta g_L^b \tag{17}$$

$$g_R^b = \left[g_R^b\right]_{ref} + \frac{1}{3}\delta s^2 + \delta g_R^b. \tag{18}$$

It is possible to simplify the parameter dependence of observables that contain Γ_b and A_b by choosing a convenient rotation in δg_L^b-δg_R^b space. This defines two new parameters ξ_b and ζ_b,

$$\xi_b = \delta g_L^b \cos\phi_b - \delta g_R^b \sin\phi_b \tag{19}$$

$$\zeta_b = \delta g_L^b \sin\phi_b + \delta g_R^b \cos\phi_b, \tag{20}$$

where the rotation angle is chosen to be $\phi_b = \tan^{-1}|g_R^b/g_L^b| \simeq 0.181$. The $Z \to b\bar{b}$ partial width and asymmetry parameter now depend upon two parameters each, $\Gamma_b = \Gamma_b(\xi_b, \delta s^2)$ and $A_b = A_b(\zeta_b, \delta s^2)$.

The result of fitting $\xi_b, \zeta_b, \delta s^2$ linear expansions to the current average values of several ξ_b dependent observables (σ^0_{had}, R_ℓ, R_b, and R_c), ζ_b dependent variables (A_b and A^b_{FB}), and leptonic $\sin^2\theta_W^{\rm eff}$ measurements is shown in Figures 21 and 22. Figure 21 shows the ξ_b-δs^2 plane and Figure 22 shows the ζ_b-δs^2 plane. The measured observables define the bands shown in both plots. The results of the fit are shown as 68.3 % elliptical contours and the MSM regions for $m_t = 174.1 \pm 5.4$ GeV and 70 GeV $< m_H <$ 1 TeV are also shown.

The 68% confidence region in $\delta\sin^2\theta_W^{\rm eff}$-$\xi_b$ space preferred by the fit deviates somewhat from the MSM region but is consistent statistically with the MSM. The 68% confidence region in $\delta\sin^2\theta_W^{\rm eff}$-$\zeta_b$ space preferred by the fit manifests the 2.9 σ discrepancy with the MSM that was noted in Section 6.3.2. The ζ_b fit illustrates the inconsistency of the SLD A_{LR} result and the LEP A^b_{FB} results. If both measurements are correct, then A_b (ζ_b) must deviate from the MSM. The direct A_b measurement from SLD is consistent with an anomalous A_b but is not yet precise enough to be significantly inconsistent with the MSM. More precision is required to understand if the SLD-LEP $\sin^2\theta_W^{\rm eff}$ discrepancy has a physical origin in an anomalous value of A_b.

6.3.4 Future Heavy Flavor Electroweak Measurements

The precision of future heavy-flavor electroweak measurements is summarized in Table 4. It is clear that the precision of the SLD A_b measurement will approach the LEP average when the 1998 data are fully analyzed and a fourth technique based upon vertex charge is implemented. This technique is self-calibrating and should provide precision that is comparable to the jet

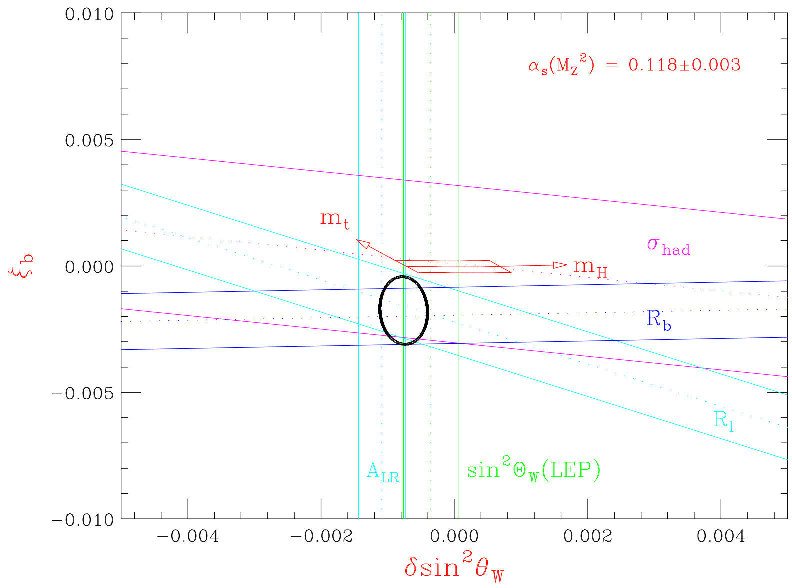

Figure 21: The 68% confidence bands determined by several observables are plotted in the $\delta\sin^2\theta_W^{\rm eff}$-$\xi_b$ plane. The 68% confidence region determined by the best fit is shown as the ellipse. The MSM region is shown as the parallelogram.

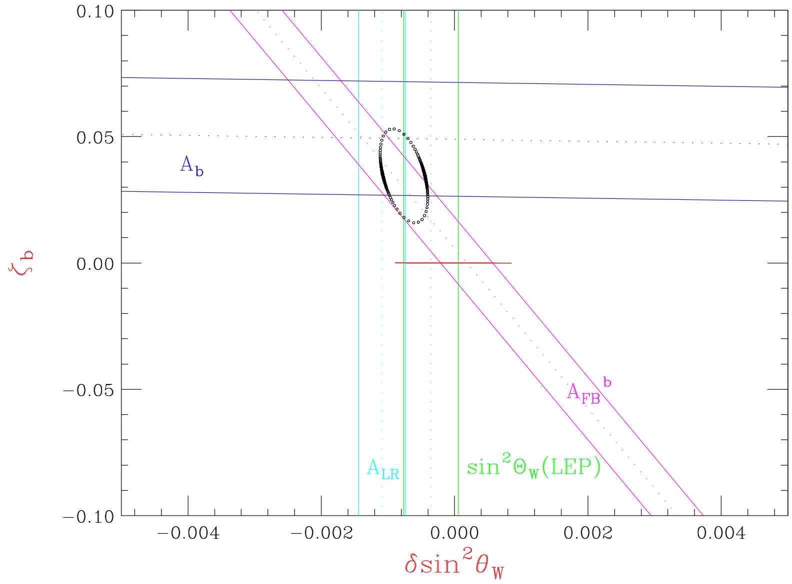

Figure 22: The 68% confidence bands determined by several observables are plotted in the $\delta\sin^2\theta_W^{\rm eff}$-$\zeta_b$ plane. The 68% confidence region determined by the best fit is shown as the ellipse. The MSM region is shown as the line.

charge technique. The overall result would reach the ± 0.02 level with a 1 million Z sample. The 1 million event sample would lead to measurements of R_b, R_c, and A_c with precisions of ± 0.001, ± 0.005, and ± 0.024, respectively. The R_b measurement would be the best single measurement of its kind. The measurement of R_c would be more precise than the current LEP average. The measurement of A_c is already equal to the LEP average and would exceed it (significantly).

Table 4: Current and projected precision of various electroweak observables.

Observable	Now	1998 Final	1MZ Projected	Current LEP
R_b	± 0.0020	± 0.00125	± 0.00094	± 0.00076
R_c	± 0.011	± 0.007	± 0.0052	± 0.0048
A_b	± 0.036	± 0.026	± 0.020	± 0.022
A_c	± 0.040	± 0.034	± 0.024	± 0.040

6.4 Summary of SLD Electroweak Measurements

The SLD measurement of A_{LR} has consistently produced a determination of $\sin^2\theta_W^{\rm eff}$ that is smaller than the one measured by the LEP Collaborations and is only marginally consistent with the Minimal Standard Model. The technique used is extremely robust and free of systematic uncertainties. The most precise of the LEP $\sin^2\theta_W^{\rm eff}$ determinations are the measurements of the b-quark forward-backward asymmetries which are the most discrepant with the SLD result. The discrepancy has several possible sources: it is possible that the A_{LR} measurement is incorrect, it is possible that the A_{FB}^b measurements are incorrect, or it is possible that A_b deviates significantly from the MSM value which would distort the interpretation the A_{FB}^b measurements. At the current time, the direct SLD measurement of A_b suggests that this last explanation is favored, however, it is not precise enough to be definitive. It is clear that the more precise A_{LR} and A_b measurements that could be made with an expanded Z sample would do much to understand the nature of this important problem.

We have already seen in Section 6.2.2 that the Higgs mass sensitivity of the current world average $\sin^2\theta_W^{\rm eff}$ measurement is already better than future M_W measurements at LEP and the Tevatron will provide. The proposed SLD measurement would produce a determination of $\log(m_H)$ that would be a factor of two better than the future M_W measurements will provide. It is clear that performing the best possible measurements of both $\sin^2\theta_W^{\rm eff}$ and A_b will be crucial and longlasting contributions to electroweak physics.

7 B Physics

7.1 B_s^0 Mixing

7.1.1 Introduction

With a 1 MZ data set, the SLD Collaboration has the opportunity to observe the time dependence of $B_s^0 - \bar{B}_s^0$ mixing for the first time, and to measure the oscillation frequency Δm_s. The experiment is sensitive to precisely those values of Δm_s favored by theory, insuring that we will either observe a mixing signal or set a very interesting limit. The measurement of Δm_s will have significant implications. It will allow the first accurate determination of the CKM element which is least well-known, $|V_{td}|$. In conjunction with previous measurements of $|V_{ub}|$ and $|V_{cb}|$ this will determine the sides of the unitarity triangle, and provide the best information on the angle γ for years to come. An accurate measurement of $|V_{td}|$ will thus allow a determination of the phase of the mixing matrix *that is independent of the constraint from CP violation* in the kaon system. This would put Kobayashi and Maskawa's conjecture [16], that the CKM phase accounts for CP violation, to its first experimental test and set the stage for the coming studies of CP violation in the B meson system.

If Δm_s is beyond the SLD's reach, it will still be possible to set a limit which will significantly constrain, and essentially determine, the Wolfenstein parameters ρ and η in a Standard Model analysis (due to the rather small remaining allowed region in the SM).

7.1.2 B_s^0 Mixing Determines $|V_{td}|$ and More

Neutral B mesons mix by virtue of second order weak interactions. In the Standard Model, the oscillation frequency for B_d^0 mixing is related to the CKM element $|V_{td}|$ by the box diagram calculation,

$$\Delta m_d = \frac{G_F^2}{6\pi^2}|V_{tb}|^2|V_{td}|^2 m_t^2 M_{B_d} B_d {f_{B_d}}^2 \eta_{QCD} F({m_t}^2/M_W^2). \tag{21}$$

The Bag factor B_d and decay constant f_{B_d} are as yet unmeasured. Present theoretical uncertainties [17] in these quantities propagate to a nearly thirty percent error in $|V_{td}|$ despite the fact that Δm_d is well measured: $\Delta m_d = 0.471 \pm 0.016$ ps^{-1} [18]. So B_d^0 mixing by itself determines $|V_{td}|$ but with large theoretical uncertainty.

A more accurate determination of $|V_{td}|$ is possible by measuring the ratio,

$$\frac{\Delta m_s}{\Delta m_d} = \left[\frac{\eta_{B_s} M_{B_s} {f_{B_s}}^2 B_s}{\eta_{B_d} M_{B_d} {f_{B_d}}^2 B_d}\right] \left|\frac{V_{ts}}{V_{td}}\right|^2 \tag{22}$$

since then many of the theoretical uncertainties cancel. In fact, most new physics contributions also cancel in this ratio [19] making it a theoretically robust technique for determining $|V_{td}|$. The remaining uncertainty in $|V_{td}|$ is then about eight percent [20]. Since the unitarity of the CKM matrix implies $|V_{ts}| \simeq |V_{cb}|$, and since $|V_{cb}|$ is relatively well known, a fifteen percent measurement of Δm_s suffices to determine $|V_{td}|$ to about thirteen percent, a precision far exceeding our present knowledge.

Finally, the accurate determination of $|V_{td}|$ will allow new tests of lattice QCD calculations of f_{B_d} and B_d. Having determined $|V_{td}|$ with the ratio method, the relation for Δm_d (see Eq. 21) can be inverted to find the product ${f_{B_d}}^2 B_d$. Once the decay constant f_{B_d} is measured, it will even be possible to isolate the bag factor empirically and thereby test the details of the calculations.

7.1.3 Theoretical Expectations for Δm_s

The status of our present knowledge of the magnitude of $|V_{td}|$ is conveniently represented in the familiar unitarity triangle, shown in Figure 23. The figure shows the constraints on the two Wolfenstein parameters ρ and η that derive from measurements of the CP violation parameter ϵ in K^0 decay, the value of Δm_d from measurements of B_d^0 mixing, the present limit on Δm_s, and the determination of $|V_{ub}|/|V_{cb}|$ coming from studies of the endpoint of the lepton spectrum in B semi-leptonic decay. The figure, from Paganini et al. [20], shows the allowed region for the apex of the unitarity triangle, the point (ρ,η). The length of the side of the triangle extending from (1,0) to (ρ,η) is equal to $|V_{td}|\ /\lambda|V_{cb}|$ where λ is the sine of the Cabibbo angle. The extent of the allowed region indicates the current uncertainty in $|V_{td}|$. The authors have derived the resulting constraints on Δm_s, and find that 8.1 $\mathrm{ps}^{-1} < \Delta m_s < 15.9\ \mathrm{ps}^{-1}$ with 68% CL, and that $\Delta m_s < 21\ \mathrm{ps}^{-1}$ at 95% CL. While the assignment of strict confidence intervals to theoretical errors is risky business, it is clear that the favored value of Δm_s is in the region of 8 to 16 ps^{-1}.

The combined LEP results exclude $\Delta m_s \leq 11.5\ \mathrm{ps}^{-1}$ at 95% CL [18]. If the theory is right, we will either observe B_s^0 mixing or set a lower limit on Δm_s that will severely restrict the allowed region for ρ and η.

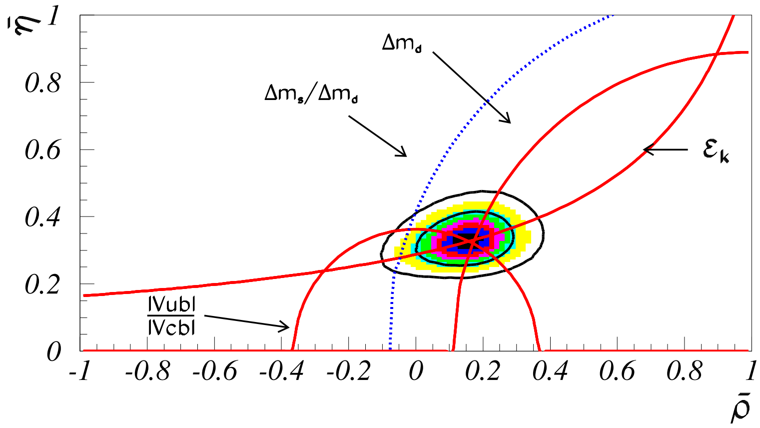

Figure 23: Allowed region for ρ and η coming from constraints imposed by measurements of $|V_{ub}|$,Δm_d, Δm_s, and ϵ.

7.1.4 SLD Mixing Measurements

The techniques for measuring the time dependence of B^0 meson mixing have undergone important refinements in the last few years, but the underlying principle is unchanged. What is required is the determination both at the time of production and at the time of decay whether the meson is a B^0 or its antiparticle, a $\bar{B}^0$. The other ingredient is the determination of the proper time of the decay, which follows from measurements of the B^0 decay length and the B^0 energy. B^0 mixing materializes as a sinusoidal oscillation in flavor as a function of proper time:

$$P[B^0(t=0) \to B^0(t)] = \frac{1}{2\tau_B} e^{-t/\tau_B} (1 + \cos \Delta m t) \tag{23}$$

$$P[B^0(t=0) \to \bar{B}^0(t)] = \frac{1}{2\tau_B} e^{-t/\tau_B} (1 - \cos \Delta m t) \tag{24}$$

SLD has measured time dependence in B_d^0 mixing with four separate analyses. All the analyses use the polarization-enhanced forward-backward asymmetry in conjunction with an opposite hemisphere jet charge measurement to flavor tag the initial state. The polarization tag, which is, of course, unique to SLD, is fully efficient and very powerful, with an average correct-tag rate of 75%. Four different techniques are used to tag the flavor of the decaying B. The first uses the presence of high P_T leptons to tag the event as $Z \to b\bar{b}$, and the sign of the lepton to determine b flavor. The decay point is reconstructed using the average intercept of the lepton trajectory with other tracks in that hemisphere. The second technique exploits SLD's vertexing capability to identify a D vertex topologically among the decay products in events with a high P_T lepton. The B decay point is reconstructed by intersecting the lepton and D trajectories. This analysis is less efficient than the inclusive lepton technique, but it has superior resolution and higher tagging purity. The third and fourth methods rely heavily on SLD's excellent vertex detection to identify $Z \to b\bar{b}$ events by finding separated vertices which have invariant masses exceeding the D mass. The B flavor is determined (method 3) by identifying the sign of a charged kaon among the decay products, and assuming it results from the $b \to c \to s$ cascade. In method 4, the final state tag is derived from a measurement of the charge dipole of tracks associated with the secondary vertex. Results from the four analyses are shown in Figure 24. Figure 25 compares these SLD measurements (made with 150 kZ's and VXD2) to those of the LEP experiments (2-4 MZ's per experiment) and CDF. The statistical advantages of polarization tagging and precise vertexing are apparent.

7.1.5 Measuring B_s^0 Mixing

The time dependence of B_s^0 mixing has proven to be particularly difficult to observe because only ten percent of all B hadrons are B_s^0 mesons and because B_s^0 flavor oscillations are very rapid, near the resolving power of the detectors. Imperfect initial and final state flavor tagging compounds the difficulty. The small fraction of B_s^0 mesons in the final state means that the oscillatory signal is diluted by large backgrounds. The proper time resolution poses more fundamental limitations. Roughly speaking, the proper time resolution washes out the signal when $\sigma_t \geq \Delta m_s{}^{-1}$. This effect puts a special premium on high resolution vertex detection, and extends SLD's reach beyond that of the LEP experiments.

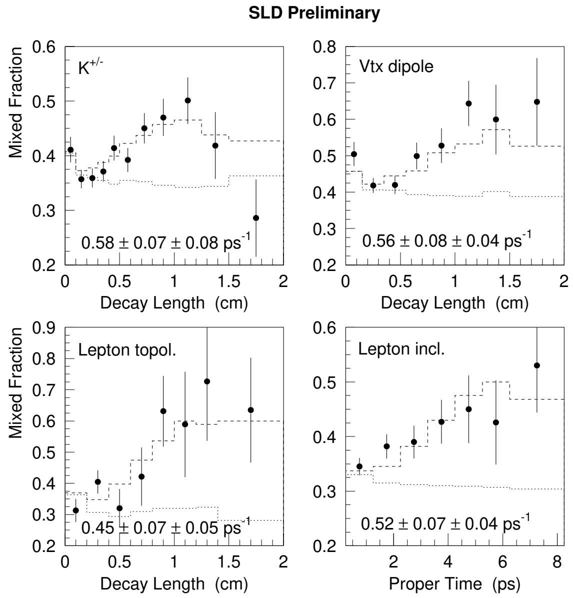

Figure 24: B_d^0 mixing measurements at SLD using four different techniques to tag the final state flavor.

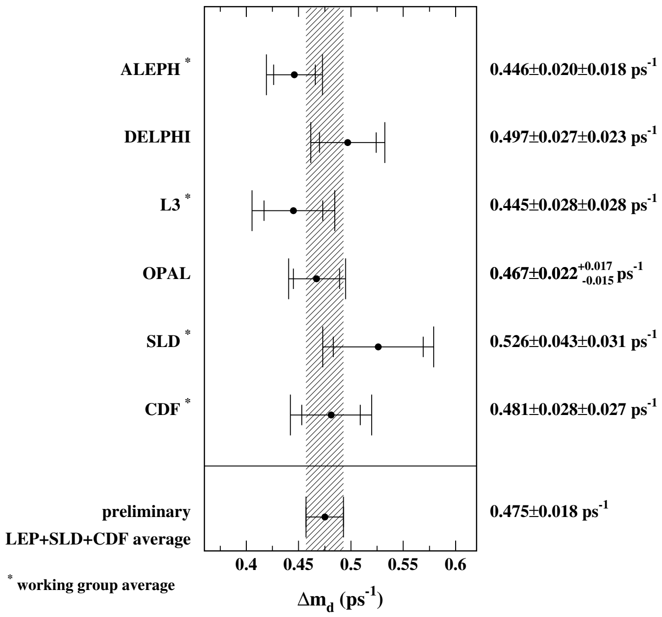

Figure 25: Current Measurements of Δm_d.

7.1.6 Current SLD Limits on B_s^0 Mixing

SLD has developed an inclusive lepton analysis, a lepton+D analysis, and a charge-dipole analysis to study B_s^0 mixing, using techniques similar to those discussed above for B_d^0 mixing measurements. The analyses have been considerably refined in order to extract more information from the data. We have developed a maximum likelihood analysis which accounts for initial and final state tagging probabilities, decay length resolution, boost resolution, and B_s sample fractions on an event-by-event basis. The present analysis uses 250 kZ's taken with VXD3 in the 1996, 1997, and Winter 1998 SLD runs. Results for the lepton+D and charge-dipole analyses are shown in Figure 26. The results are presented in terms of a Fourier amplitude A, which is introduced to modulate the cosine term in the probability density. We fit for this amplitude for a range of possible oscillation frequencies Δm. The amplitude is normalized to be equal to 1 when $\Delta m = \Delta m_s$, and is nominally 0 away from the Fourier peak. The fit also gives the error in $A(\Delta m)$, which measures the experimental sensitivity. The parameter space excluded by the present analysis is $\Delta m_s < 1.7$ ps^{-1} and $3.3 < \Delta m_s < 5.0$ ps^{-1} at the 95% confidence level.

The maximum likelihood fit has been checked on simulated data. The fitting functions accurately describe all aspects of the full simulation. The time evolution of the mixed fraction for B_s^0 mesons, for example, is shown in Figure 27 in good agreement with the fitting function. Results of a simulated 2.0 MZ experiment using only the lepton+D method are shown in Figure 28. The amplitude peaks as expected near $\Delta m_s = 10$ ps^{-1}, which was the input to the simulation.

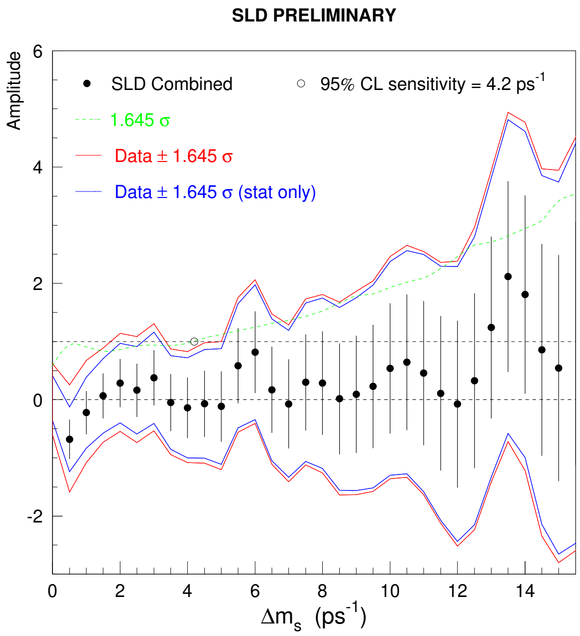

Figure 26: Measured oscillation amplitude as a function of Δm_s for the lepton+D and charge-dipole analyses combined.

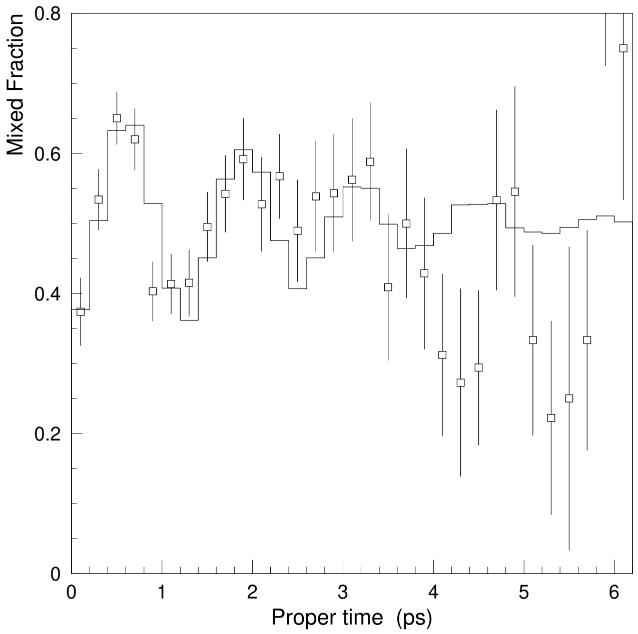

Figure 27: Mixed fraction vs. proper time for a pure B_s^0 sample in the lepton+D analysis. Simulated data is given by the points with error bars; the fitting function is shown as the histogram. The input value of the mixing parameter was $\Delta m_s = 5$ ps^{-1}.

SLD is ideally suited for the measurement of B_s^0 mixing, having superb decay length resolution, pure and efficient flavor tagging, and Cherenkov particle identification to enhance the fraction of B_s^0 mesons. The decay length resolution provided by the new vertex detector is foremost among these. Figure 29 shows this resolution for the lepton+D technique. At about 90 microns it is two to three times better that at LEP. It is coupled to boost resolution, also shown in the Figure, which matches world standard. The resulting proper time resolution is 0.05 ps at short proper times.

Flavor tagging the initial and final states is also important. Moser [21] has quantified how the significance of a B_s^0 mixing measurement depends on the mistag rate, η:

$$S \propto f_{B_s}(\eta)\,(1-2\eta) \tag{25}$$

Note that the B_s^0 fraction, f_{B_s}, implicitly depends upon η. The significance of events with very pure initial and final state tags will far exceed those with average purities. By virtue of beam polarization, SLD has a unique, fully efficient, and very pure initial state tag that can be used in combination with more traditional techniques (lepton tagging, jet-charge tagging), vertex-based methods (vertex charge tagging, dipole charge tagging), or kaon tagging. The resultant inclusive tag, affectionately dubbed the "kitchen sink", has world-record performance as shown in Figure 30. Note the sizable fraction of events with purities above 90%. Final state tagging is also of very high purity, enhanced by use of vertex information, lepton P_T or kaon identification. Figure 31 shows the purities in the lepton+D analysis mentioned above.

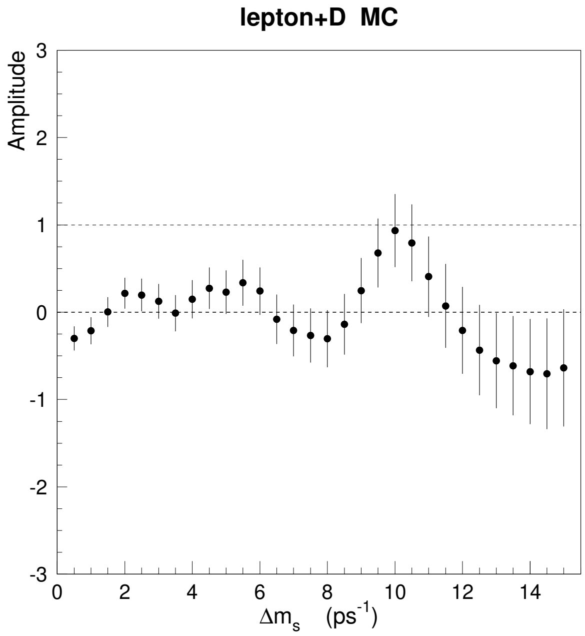

Figure 28: Amplitude vs.$\Delta m_s$for the lepton+D analysis in simulated data. The input value was $\Delta m_s = 10$ ps^{-1}.

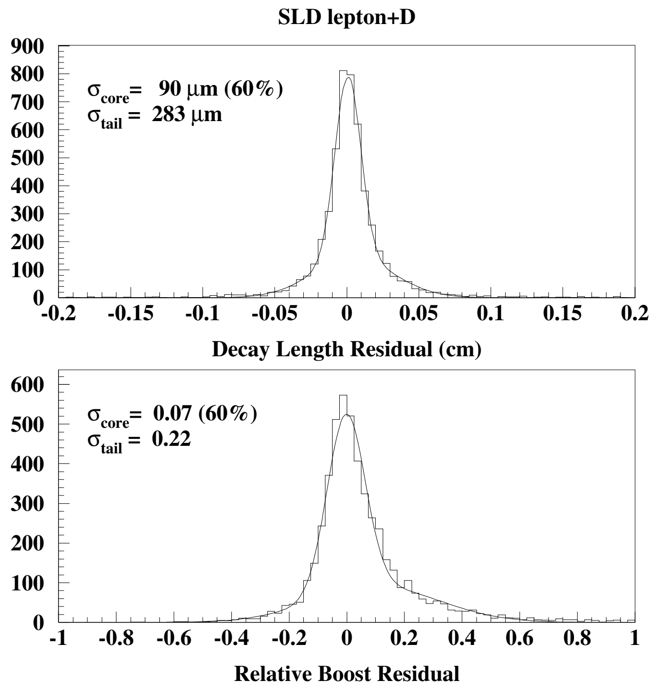

Figure 29: Upper figure: Decay length resolution in the lepton+D method.Lower figure: boost resolution.

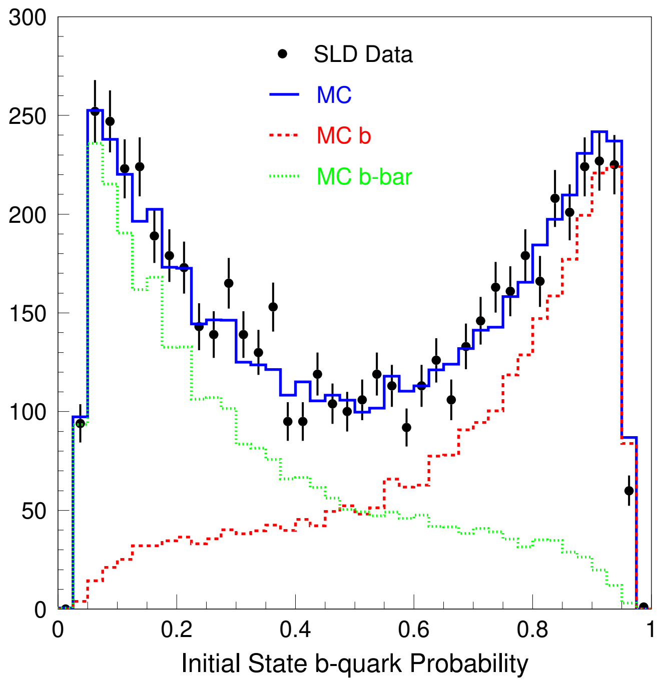

Figure 30: Purity distribution for the inclusive initial state tag in the charge-dipole analysis.

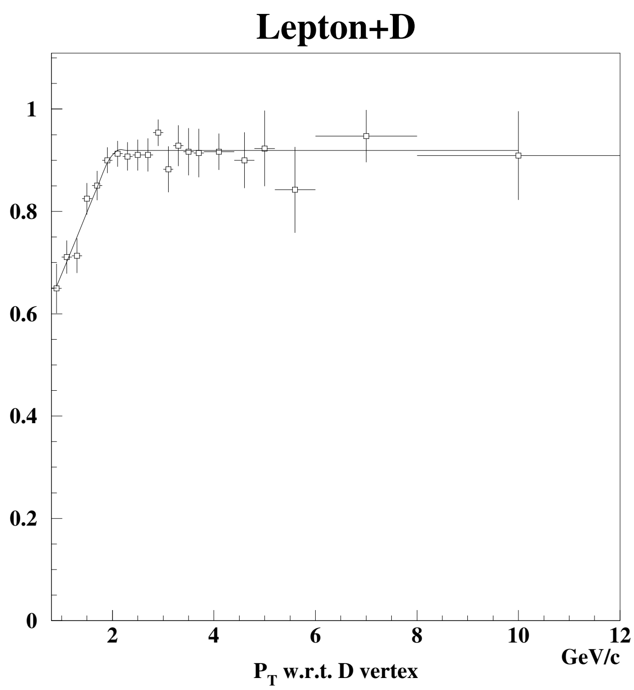

Figure 31: Fraction of direct leptons ($b \to \ell$) from B_s^0 decays in the lepton+D analysis.

Enhancing the B_s fraction obviously improves the size of the mixing signal relative to background. In SLD, we have several techniques for doing so. As mentioned above, improvements in tagging purity result in improvements in the B_s fraction. In addition, by identifying fragmentation kaons, produced in association with a B_s^0 meson, or kaons associated with D_s or D_s^{**} decays, we can enhance the B_s^0 fraction. Finally, by reconstructing D_s mesons among the B decay products, we enhance the probability the parent was a B_s^0.

7.1.7 Experimental Reach for B_s^0 Mixing with 1 MZ

The current SLD limits on Δm_s provide a solid basis for estimating the reach of the experiment with a 1 MZ data sample. Extrapolating the sensitivity of the current analyses to the larger data set is simply a matter of scaling the current significance by $\sqrt{1,000,000/250,000}$. Improvements in the analysis, discussed below, extend the reach beyond this simple extrapolation. Significant improvements to our sensitivity come by including new analyses to the three mentioned above. We are currently developing an analysis based on exclusive reconstruction of D_s mesons. The presence of a D_s meson among the B decay products enhances the B_s fraction in the sample, and the charge of the meson tags the B flavor at decay. The D_s mass peak observed in the 1996-1998 data is shown in Figure 32. Decay length resolution for this mode is very good (75 μm), because the D_s trajectory can be included with the other B decay tracks in determining the decay vertex position. Figure 33 shows a reconstructed 1998 event which is a candidate for a $B_s^0 \to \bar{B}_s^0 \to D_s^+ \ell^- \bar{\nu}_\ell$ decay. We estimate the significance for this mode using the formulae developed by Moser and Roussarie [21]. Input parameters we have assumed for this analysis are given in Table 5. The enhancement factor listed in the table accounts for the difference in calculating the significance with average values of the mistag rate and B_s fraction, and that where these quantities are calculated event by event. As a cross-check, we have confirmed that the significance evaluated with this formula agrees with that from the full maximum likelihood fit in the lepton+D analysis.

Table 5: Parameters for Moser formula evaluation of B_s^0 mixing significance.

Parameter	$\ell + D$	D_s	ℓ+K/ℓ+ϕ
Reconst. Eff.	0.031	0.0039	0.0033
B_s Fraction	0.153	0.244	0.257
Mistag Rate	0.21	0.26	0.256
Decay Len. Res.			
Cone [μm] (frac)	90 (60%)	75 (60%)	94 (60%)
Tail [μm]	283	380	340
Boost Resolution			
Core (frac)	0.067 (60%)	0.067 (60%)	0.067 (60%)
Tail	0.21	0.21	0.21
Enhancement Factor	1.20	1.20	1.20

Other analyses are also under development. By tagging $\ell^{\mp} K^{\pm}$ events, we preferentially

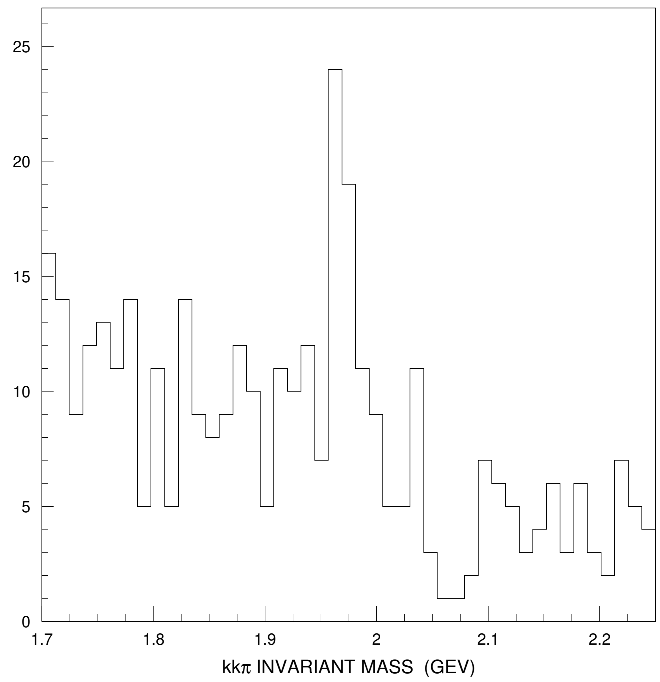

Figure 32: Invariant mass of $KK\pi$ in 1996-98 SLD data.

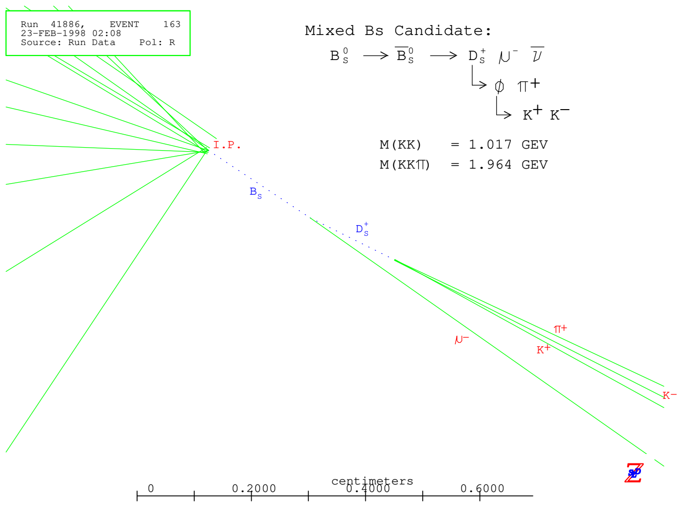

Figure 33: A reconstructed 1998 event which is a candidate for a $B_s^0 \to \bar{B}_s^0 \to D_s^+ \ell^- \bar{\nu}_\ell$ decay.

select decays of the type $B_s^0 \to \ell^+ \nu \bar{D}_s^{**}$, $\bar{D}_s^{**} \to K^- \bar{D}^0$ and $B_s^0 \to \ell^+ \nu \bar{D}_s$, $\bar{D}_s \to K^- X$. These modes have low efficiency but they have enhanced B_s fraction and excellent decay length resolution. The reach expected from these decays combined with those from $\ell\phi$ events is calculated from parameters given in the table.

Improvements in SLD tracking solid angle, lepton identification solid angle, and impact parameter resolution have already been demonstrated and will be available for future analyses. We have approximated the impact of the acceptance improvements by boosting lepton acceptance by 15%, a value derived from recent data analyses. Separate studies lead us to expect a 20% improvement in the decay length resolution from the improved impact parameter resolution. A re-evaluation of the amplitude fit with reduced decay length errors leads to an additional increase in the significance which varies with Δm_s. We scale significances by the product of these factors.

SLD's B_s^0 mixing reach is shown in Figure 34 for a 1 MZ data sample. In the absence of a signal, we would expect to set a 95% CL that $\Delta m_s \geq 20$ ps^{-1}. This sensitivity significantly exceeds that coming from the present LEP analyses, $\Delta m_s \geq 12.9$ ps^{-1} at 95% CL. We could see a 2.5 σ amplitude excursion up to $\Delta m_s = 15$ ps^{-1}. SLD has the potential to discover a significant B_s^0 mixing signal precisely at the values of Δm_s favored by theoretical analysis.

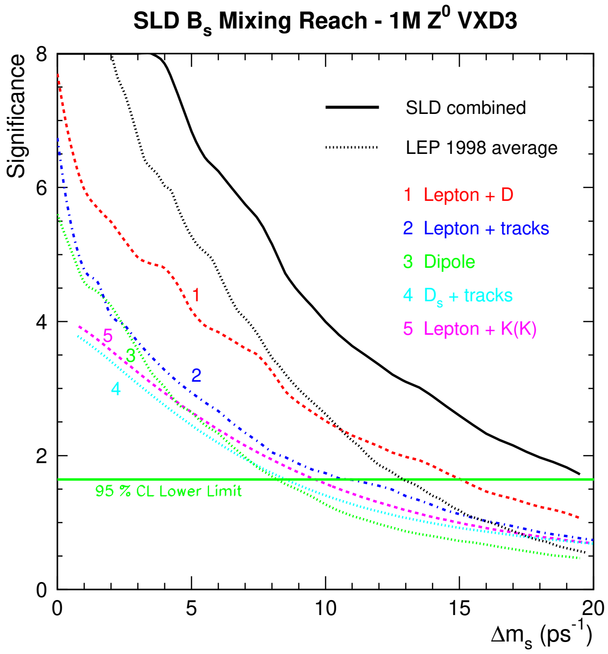

Figure 34: The B_s^0 mixing signal significance as a function of Δm_s for a 1 MZ data sample.

7.1.8 Future Determinations of $|V_{td}|$

If we are to overconstrain the CKM matrix and test the Standard Model explanation of CP violation, a precise measurement of $|V_{td}|$ is essential.

The measurement of the oscillation frequency Δm_s in B_s^0 mixing will likely provide the most accurate and theoretically robust determination of $|V_{td}|$. Were it not for theoretical uncertainties, B_d^0 mixing would be the perfect way to measure $|V_{td}|$. The measurement of $\Delta\Gamma$, the difference in lifetimes of the two mass eigenstates in the B_s^0 system, also determines Δm_s. But uncertainties in the factor relating $\Delta\Gamma$ and Δm_s adds uncertainty to the extraction of $|V_{td}|$ [22]. Measuring the ratio of B radiative decay rates $\Gamma(B \to \rho\gamma)/\Gamma(B \to K^*\gamma)$ also determines $|V_{td}|/|V_{ts}|$. Theoretical uncertainties in the hadronic form factors and long distance effects hamper efforts to extract $|V_{td}|$ reliably in this case [23]. The branching ratio for the process $K \to \pi\nu\bar{\nu}$ is sensitive to $|V_{td}|$ and is not plagued with theoretical complications[23]. But this process looks beyond present experimental reach. B_s^0 mixing is the preferred technique.

CDF and HERA B will certainly explore B_s^0 mixing. In its present incarnation, HERA B doesn't have sufficient vertex resolution to explore beyond $\Delta m_s = 11$ ps^{-1}. CDF advertises sensitivity to $\Delta m_s \leq 24$ ps^{-1} if luminosity and trigger upgrades are successful in Run II at the Tevatron. In any case, it will be well into the new Millennium before results are forthcoming. Establishing a convincing signal for B_s^0 mixing may require coincident results from two or more experiments.

SLD will either measure or place interesting constraints on B_s^0 mixing as soon as it can collect the required luminosity. The necessary tools work extraordinarily well. The method is demonstrated. SLD is uniquely positioned for an important measurement given a modest investment in running time.

7.2 Other B Physics

7.2.1 Introduction

With one million Z decays to study, SLD will be able to contribute to many questions of topical interest in B physics, including B lifetimes, the semi-leptonic branching ratio puzzle, the search for $B \to sg$, as well as searches for rare decays. The raw number of B decays available at SLD is not competitive with LEP or the B-Factories. But the facts that $Z \to b\bar{b}$ produces all hadronic B species, separates the decay products of the b-quarks into distinct jets, and boosts them so there is very high acceptance for all particles gives the Z-Factories distinct advantages over the B-Factories. SLD's ability to efficiently flavor tag b-events and to untangle various decay topologies gives it an important niche among the Z-Factory experiments. The full power of SLD's impressive tool kit has not been thoroughly explored. It is likely to open new physics possibilities.

7.2.2 B Lifetimes

SLD has measured the B^0 and B^+ meson lifetimes inclusively by topologically identifying b-decays, then separating neutral and charged samples on the basis of the net charge of the tracks associated with the secondary vertex. Bigi, et al. expect $\tau(B^+) > \tau(B^0)$,though the 5% expected lifetime difference is much smaller than in the charm sector. SLD's analysis of its 1993 to Winter 1998 data gives the lifetime ratio $\tau(B^+)/\tau(B^0) = 1.061 \pm 0.040$. With 1 MZ the error in the ratio would drop to ± 0.023, essentially determining world average, and small enough to see the expected effect. Superb tracking and vertex resolution make the analysis possible, and unique.

7.2.3 The Puzzle of B Semi-Leptonic Decays

The B semi-leptonic branching rate is measured to be significantly below theoretical expectation. This could be because the double charm production rate ($b \to c\bar{c}s$) is enhanced beyond naive expectation, or because new physics (e.g., $b \to sg$) increases the total, but not the semi-leptonic width. The experimental situation at present is murky, with no definitive measurements of $\mathrm{B}(B \to noD)$ or $\mathrm{B}(B \to D\bar{D}X)$. SLD's tools are natural for attacking this problem, since the signature for $B \to noD$, i.e. that all tracks arise from a single B decay vertex, requires excellent vertexing resolution, and identification of "wrong-sign" D mesons from B decay requires excellent initial- and final-state flavor tags and also benefits from good kaon identification. We have begun studying these measurements. A preliminary analysis predicts we can measure $\mathrm{B}(B \to D\bar{D}X)$ with an error $\pm .025$, to be compared to the current world average $\mathrm{B}(B \to D\bar{D}X) = .05$.

7.2.4 Does $b \to sg$?

Using the high precision vertexing and particle identification capabilities of SLD, we have developed a very effective analysis to search for $b \to sg$ through high P_t $K^\pm$ production in B decays where all tracks are required to be compatible with a "single vertex" hypothesis. This analysis could establish a 95% CL upper limit on the branching ratio at about 2.5% with 1 MZ event sample which would eliminate this new physics possibility as the source of the semi-leptonic puzzle mentioned above.

7.2.5 Rare B Decays

Theoretically, the two body decays $B^0 \to \rho^0\pi^+$ and $B^+ \to K^{*0}\pi^+$ are expected to be quite rare, with branching ratios $\leq 10^{-5}$. The Delphi experiment has reported a few events at the few $\times 10^{-4}$ level, which has since been contradicted by CLEO. SLD's vertex detection permits a very efficient and background-free search. With a million Zs, we could set limits at the few $\times 10^{-5}$ level and potentially resolve the CLEO/DELPHI discrepancy.

7.2.6 Bread and Butter

SLD could well be a B-physics thesis factory with a million Z data set. It will be possible to measure the lifetimes of other B hadrons, including B baryons and B_s mesons. Inclusive properties of B decays could be cataloged: decay multiplicities; yields of pions, kaons, and leptons; transverse momentum spectra for various particles; yields of D^0, D^+, D_s, and Λ_c. B_s meson production can be studied: correlations of B_s mesons with fragmentation kaons can be measured; B_s yields determined; B_s^{**} production studied; and inclusive decays of the B_s evaluated. Precision measurements of the CKM matrix element $|V_{cb}|$ are also possible.

7.2.7 Dessert

We have begun thinking about the more exciting physics opportunities which are opened by a large statistics SLD data set. We will search for $B \to \tau\nu$ and measure $D_s \to \tau\nu$ to derive measures of the meson decay constants and $|V_{ub}|$. We have already begun studies of inclusive CP violation, as suggested by Dunietz. Hewett has raised the possibility of searching for $b \to sg$ in three-jet events, $Z \to b^*b \to sgb$. Studies of flavor changing neutral currents are possible by searching for $Z \to b\bar{s}$. The decay $B \to X_s\nu\bar{\nu}$ is expected at the 0.5×10^{-4} level, and may be accessible with SLD's particle identification and vertexing. SLD is perfectly equipped to search for anomalous topologies in B decays.

8 QCD Physics

8.1 Introduction

The Standard Model has provided a remarkably successful description of almost all available data involving the electroweak interactions. Recently, however, some measurements of the quantities R_b and A_b have been reported that are in mild disagreement, at the 2-3 standard deviation level, with Standard Model expectations. Since, on general grounds, one expects new high-mass scale dynamics to couple to the massive third-generation fermions, these measurements in the b-quark sector have aroused considerable interest and speculation. This provides motivation to study the strong-interaction dynamics of the b-quark via study of $Z^0 \to b\bar{b}g$ events.

We have started a program of measurements of the strong-interaction dynamics of the b-quark, both as a cross-check and complement to the electroweak studies, and as a laboratory for possible new effects, which theoretical prejudice suggests might couple most strongly to the third generation. Specifically, we will measure:

- The rate of gluon emission in $b\bar{b}$ events, compared with that in $c\bar{c}$ and light-quark events.
- The gluon energy and polar-angle distributions in $b\bar{b}g$ events.
- Symmetry tests in $b\bar{b}g$ events that exploit the polarised electron beam. These include checks on parity-violation at the $b\bar{b}g$ vertex, as well as a search for both CP-even and -odd, T-odd, final-state interactions.

With a 1M Z^0 event data sample to exploit the potential of VXD3 for heavy-quark tagging in a multijet environment, the relevant parameters can be measured at the few per cent level. The symmetry tests cannot be made at LEP to comparable precision due to the lack of beam polarisation.

In addition, we shall measure:

- The fractional cross sections for gluon splitting into $b\bar{b}$ and $c\bar{c}$. These have not been measured accurately at LEP.

• The fragmentation functions for b- and c-quarks to produce, respectively, B and D hadrons.
Beyond their fundamental interest in terms of QCD, these quantities are required to be known accurately so as to constrain the backgrounds to possible new physics signals in multijet events containing heavy quarks that will be produced at the TeVatron and at the LHC.

Finally, a 1M Z^0-event data sample exploiting VXD3 for light- vs. heavy-quark event separation as well as gluon jet isolation, combined with the polarised forward-backward asymmetry tag for quark vs. antiquark jet separation, and the SLD CRID particle identification, will allow the last chance for precise empirical study of jet fragmentation. The TeVatron and LHC experimental environments and detectors will not allow clean measurements of identified hadron species in both light- and heavy-, quark- and antiquark-jets, as well as gluon-jets. These measurements are of fundamental interest, and will constrain the models of fragmentation that are widely-used at today's energies. These model predictions will by necessity be extrapolated into the high-jet-energy domain for use at the TeVatron and the LHC, as well as for modelling light-quark backgrounds at the future Linear Collider.

8.2 Test of the Flavour-Independence of Strong Interactions

In order for QCD to be a gauge-invariant renormalisable field theory it is required that the strong coupling α_s be independent of quark flavor. This basic *ansatz* can be tested directly in e$^+$e$^-$ annihilation by measuring the strong coupling in events of the type $e^+e^- \rightarrow q\bar{q}(g)$ for specific quark flavors q. Whereas an absolute determination of α_s using such a technique is limited, primarily by large theoretical uncertainties, to the 5%-level of precision, a much more precise test of the flavor-independence can be made from the ratio of the couplings for different quark flavors, in which most experimental errors and theoretical uncertainties are expected to cancel. Furthermore, it has recently been suggested [24] that the emission of gluon radiation in $b\bar{b}$ events is expected to be modified relative to that in $q_l\overline{q_l}$ events due to the large b-mass, and that comparison of the rates for $b\bar{b}g$ and $q_l\overline{q_l}g$ production may allow measurement of the running b-mass $\overline{m_b}(M_{Z^0})$. Finally, in addition to providing a powerful test of QCD, such measurements allow constraints to be placed on physics beyond the Standard Model. For example, a flavor-dependent anomalous quark chromomagnetic moment would modify [25] the emission rate of gluons for the different quark flavors, and would manifest itself in the form of an apparently flavor-dependent strong coupling.

Using our 1993-95 data sample and a topological-vertex-mass based flavour-tag, we have measured [26]:

$$\begin{aligned}
\alpha_s^c/\alpha_s^{uds} &= 1.037 \pm 0.043(stat.)^{+0.044}_{-0.044}(syst.) \pm 0.017(theory) \\
\alpha_s^b/\alpha_s^{uds} &= 1.001 \pm 0.017(stat.)^{+0.027}_{-0.039}(syst.)^{+0.013}_{-0.016}(theory)
\end{aligned}$$

A preliminary study of the 1996 VXD3 data sample yields a statistical error of $\Delta\alpha_s^b/\alpha_s^{uds} \simeq 0.019$, implying that, even with no improvement in flavor-tagging technique, a statistical error of 0.004 is achieveable with a 1M event sample. Under the assumption of a flavour-independent strong coupling this precision translates into a measurement error of roughly

0.25 GeV/c^2 on the running b-mass $\overline{m_b}(M_{Z^0})$.

8.3 Gluon Distributions in $b\overline{b}g$ Events

In addition to the overall probability for gluon emission in $b\bar{b}$ events, one can study the structure of such emission. We have used the SLD VXD to select $Z^0 \rightarrow b\overline{b}g$ events, and to identify in each event the jets containing the B hadrons, and hence to tag the gluon jet. We have measured [28] the distributions of the gluon jet energy and the gluon polar angle with respect to the electron beam direction, and have compared our measurements with the predictions of perturbative QCD.

In addition, we have investigated possible beyond-Standard Model effects. The chromomagnetic moment of the bottom quark is induced at the one-loop level in QCD and is of the order α_s/π. One can also write down an *ad hoc* Lagrangian [25] with a $b\overline{b}g$ coupling modified via anomalous chromoelectric and chromomagnetic moments:

$$\mathcal{L}^{b\overline{b}g} = g_s \overline{b} T_a \{\gamma_\mu + \frac{i\sigma_{\mu\nu}k^\nu}{2m_b}(\kappa - i\tilde{\kappa}\gamma_5)\} b G_a^\nu \tag{26}$$

where g_s is the strong charge, T_a are the $SU(3)_c$ generators, m_b is the bottom quark mass, k is the outgoing gluon momentum, and κ and $\tilde{\kappa}$ parameterize the anomalous chromomagnetic and chromoelectric moments, respectively, which might arise from physics beyond the Standard Model. The effect of the former on three-jet observables has been calculated recently [25, 27]; non-zero values of κ would modify the gluon energy distribution in $b\overline{b}g$ events. The latter is CP-violating.

With the 1993-95 data sample we have set limits on the anomalous chromomagnetic moment κ. We find $-0.15 < \kappa < 0.09$ at 95% c.l. (preliminary); there are currently no other limits on this quantity. With 1M events and VXD3 we expect to be able to set a limit of $|\kappa| < 0.04$. We also plan to exploit b vs $\overline{b}$ jet tagging and expect to set a limit on the CP-violating chromoelectric moment of $|\tilde{\kappa}| < 0.06$.

8.4 Symmetry Tests using $b\overline{b}g$ Events

New tests of parity-violation in strong interactions have recently been proposed [29] using angular distributions in polarised $e^+e^- \rightarrow q\overline{q}g$ events. Consider the polar-angle distribution of the quark direction w.r.t. the electron beam:

$$\frac{d\sigma}{d\cos\theta} \quad \propto \quad (1 - P_{e^-} \cdot A_e)(1 + \alpha\cos^2\theta) + 2A_P(P_{e^-} - A_e)\cos\theta, \tag{27}$$

where P_{e^-} is the signed electron beam polarization, A_e (A_f) is the parity-violating electroweak coupling of the Z^0 to the initial (final) state, given by $A_i = 2v_i a_i/(v_i^2 + a_i^2)$ in terms of the vector v_i and axial-vector a_i couplings, and A_P characterises the degree of parity violation. One can write $A_P = A_q \cdot A_\theta^{QCD}$, where the second factor modulates the tree-level electroweak parity violation and can be calculated in QCD [29]. Similarly, one can consider the distribution of the azimuthal-angle χ between the event plane and the quark-electron-beam plane:

$$2\pi\frac{d\sigma}{d\chi} \quad \propto \quad (1 - P_{e^-}\cdot A_e)(1+\beta\cos 2\chi) - \frac{\pi}{2}A'_P(P_{e^-} - A_e)\cos\chi, \tag{28}$$

and $A'_P = A_f \cdot A^{QCD}_\chi$. Given the value of the electroweak parameter A_f, measurement of the angular asymmetry parameters A_P and A'_P in polarised $Z^0 \rightarrow$q$\overline{\text{q}}$g events allows one to test the QCD predictions for A^{QCD}_θ and A^{QCD}_χ, as well as set limits on parity-violation at the q$\overline{\text{q}}$g vertex.

A differential cross-section can also be constructed in terms of the polar angle ω of the vector $\bar{n}$ normal to the event plane w.r.t. the electron beam direction, where $\cos\omega$=$\sin\theta\sin\chi$:

$$\frac{d\sigma}{d\cos\omega} \quad \propto \quad (1 - P_{e^-}\cdot A_e)(1+\gamma\cos^2\omega) + 2A_T(P_{e^-} - A_e)\cos\omega. \tag{29}$$

The term linear in cosω is T-odd and is proportional to the parameter A_T. The vector normal to the event plane can be defined in two ways: 1) the three jets are ordered according to their energies, and the two highest energy jet momenta are used to define $\bar{n} = \vec{p}_1 \times \vec{p}_2$; and 2) the quark and anti-quark momenta are used to define $\bar{n} = \vec{p}_q \times \vec{p}_{\bar{q}}$. The asymmetry term is CP-even in the first definition, and CP-odd in the second. The first definition does not require jet flavor identification, and we have measured the asymmetry for inclusive hadronic Z^0 decays [30]. The second definition requires tagging both quark- and antiquark-jets. In both cases, in the Standard Model the asymmetry vanishes identically at tree level, but higher-order processes yield non-zero contributions for e$^+$e$^-$ $\rightarrow b\bar{b}g$. However, due to various cancellations, these contributions are found to be very small at the Z^0 resonance and yield values of the asymmetry parameter $|A_T| \sim 10^{-5}$ [31]. Measurement of these asymmetries are hence potentially sensitive to physics processes beyond the Standard Model [32].

Using the 1993-97 data sample we have set [33] a 95% c.l. limit on parity-violation at the $b\bar{b}g$ vertex of $|\Delta A^{QCD}_\theta| < 0.12$, on CP-even T-odd final-state interactions of $|A^+_T| < 0.04$ and on CP-odd T-odd final-state interactions of $|A^-_T| < 0.06$ (preliminary). The corresponding limits with a 1M Z^0 sample are at the per cent level: 0.04, 0.01 and 0.01, respectively.

8.5 Measurements of the g $\rightarrow c\bar{c}$ and g $\rightarrow b\bar{b}$ Cross Sections

The $g \rightarrow q\bar{q}$ vertex is the QCD analog of the $\gamma \rightarrow e^+e^-$ vertex in QED. QCD predicts events of the type $Z^0 \rightarrow q\bar{q}g$, with $g \rightarrow c\bar{c}(b\bar{b})$ in about 2% (0.3%) of hadronic events. Heavy pairs are not expected to be produced in the fragmentation process. Two limited measurements of each of these cross sections have been made by the LEP experiments: σ(q$\overline{\text{q}}$ $c\bar{c}$) has been measured with a 25% relative error, and σ(q$\overline{\text{q}}$ $b\bar{b}$) with a 40% relative error. Limited knowledge of the latter now causes the dominant systematic error in the best measurements of R_b and is hence restricting the window on possible new physics in that sector.

We have made a preliminary study using the 1993-6 data sample and a similar method as DELPHI. Our efficiency for selecting 4-jet events containing g $\rightarrow b\bar{b}$ events is roughly 4 times higher with the same signal/background. With an optimised analysis to take full advantage of VXD3, and a 1M Z^0 sample, our measurement should be the world's best. As part of this analysis program we also expect to be able to set the world's best limit on light-gluino production via $g \to \tilde{g}\tilde{g}$.

8.6 Jet Fragmentation Studies

8.6.1 Heavy-Quark Fragmentation

The types and energy distributions of heavy hadrons produced in Z^0 decays are interesting both as tests of theories and fragmentation model, and as input to heavy flavor physics analyses. We have recently published a competitive measurement of the shape of the B-hadron energy distribution by reconstructing the energies of individual semi-leptonic B-hadron decays in our 1993-5 data sample [34]. VXD3 should improve this measurement substantially as it was limited by efficiency at low energy as well as statistics. A 1M Z^0 sample would allow us to make the definitive measurement.

We have studied the production of the charmed mesons D^+ and D^{*+}, using VXD2 to get excellent separation of primary D mesons and those from B hadron decay [39]. We already have a competitive measurement of the charmed pseudoscalar:vector meson production ratio, and statistics-limited measurements of the energy spectrum and spin alignment. A 1M Z^0 sample would allow us to make the definitive measurements of these quantities, as well as to study the production of other heavy hadrons such as D_s, Λ_c, D^{**}, etc.

8.6.2 Light-Quark Fragmentation

The hadronization process remains one of the least theoretically understood areas of high energy physics. Thus it is important to make as many precise measurements of hadronic final states as possible, not only for their fundamental interest, but also in order to test the fragmentation models that are used to simulate backgrounds to current heavy flavor measurements at the Z^0, properties of t-quark and $W^\pm$ boson decays, and backgrounds to many processes that might be studied at future colliders. The high-statistics, clean samples of $e^+e^- \to q\bar{q}$ at the Z^0 resonance will be the best source of such measurements for many years to come, so the program of study should be as complete as possible.

The LEP experiments have a rather large experimental program in this area, studying both inclusive properties of hadronic events and the production of a number of identified particles [35]. Using the high purity samples of identified particles tagged with the CRID we have made competitive measurements of the production of $\pi^\pm$, $K^\pm$, K^0, K^{*0}, ϕ, p/$\bar{\text{p}}$, and $\Lambda^0/\bar{\Lambda}^0$ production in hadronic Z^0 decays with only 150,000 Z^0 decays. In addition we have begun a program of more detailed studies, using the VXD to make the first measurements of the production of these particles in light-flavor events, giving a purer fragmentation test, as well as in b- and c-flavor events, which provide useful checks of our models of heavy hadron production and decay [36]. Also, using the beam polarization to separate light quark jets from light antiquark jets, we have made the first comprehensive study of leading particle effects [37], observing leading baryons and vector and pseudoscalar kaons at high momentum. We plan to extend these studies to include separation of quark and gluon jets, an area in which the LEP experiments have made considerable progress recently, and also to separate u jets, d jets, and s jets.

A 1M Z^0 sample would allow precise measurements of these fragmentation properties and exacting tests of theoretical and fragmentation model predictions. It would also allow us to study the production of more exotic particles such as scalar and tensor mesons, orbitally excited baryons, Ω^-, etc., which have been observed at LEP but not measured precisely.

Correlations between identified particles provide additional tests of the fragmentation process. We have begun a study that confirms that charge, strangeness and baryon number are conserved locally in the fragmentation process. We also see a strong long-range correlation in K^+K^- pairs at high momentum, as expected from leading $K^\pm$ production in $s\bar{s}$ events. The electron beam polarization allows the study of signed correlations, i.e. the measurement of whether the particle or antiparticle of a particular type follows the quark direction more strongly. A 1M Z^0 sample would allow a quantitative study of these correlations and provide additional stringent tests of fragmentation models. Putting all of this information together, we hope to learn how to tag jets of individual light flavors using high momentum identified particles. Quantifying such tags will be usful in extending our fragmentation measurements to events of all five flavors as well as for measuring the electroweak couplings of the Z^0 to the light flavors, and may find applications in other types of collisions.

A little-studied aspect of fragmentation is the polarization of particles in jets. Since Z^0 decays typically produce left-handed quarks and right-handed antiquarks, we might expect the leading particles to be longitudinally polarized. Experiments at LEP have observed such polarization in high-momentum Λ^0 and marginal signals are seen for longitudinal spin alignment of ρ, K^*, and ϕ mesons [35]. A 1M Z^0 sample would allow us to compete in this area and to extend such studies to other particles, such as Ξ^- and Ω^-. We have previously searched for jet handedness [38], a possible inclusive measure of quark polarization, the sensitivity for which is enhanced by the beam polarization. We would like to update this study to look for signals at the sub-1% level. There exist predictions for transverse polarization of e.g. Λ^0 with respect to the plane defined by the quark and Λ^0 directions, for which high statistics and a tag of the quark direction, such as is provided by the beam polarization, are needed.

Part V
Resources

9 Manpower

SLD from the very beginning has been the smallest of the large collider collaborations (the four LEP experiments, CDF, D0, etc.) Thus, manpower has always been a concern. However, we have been fortunate with the high quality, dedication, and hard work of this small collaboration. In the 1997-98 run, while more help would have been nice, the strength of the collaboration has been sufficient to do a creditable job in carrying out the experiment. We have adequately staffed the shifts for this long run. The SLD detector has run very reliably, with very little running time lost because of detector problems, and the performance of the detector is better than ever before. Both the new vertex detector, VXD3, and the polarization measurements are achieving unprecedented precision. And, equally important, the data analysis is proceeding with a very high level of competence and in a timely fashion, and the publication rate of our results cannot be faulted.

During the February 1998 SLD Collaboration meeting, we carried out a manpower survey for the proposed run extension. All of the currently active institutions expressed their interest in continuing at some level in the extended running. We then focused on an estimate of the number of students, post docs, and faculty leaving SLD and to what extent such departures would be compensated for by new students and post docs. There was some variation among the groups, with several groups expecting to move a larger fraction of their resources to other experiments. The majority of the active groups, however, expected to be able to maintain their present level of effort or even slightly increase their effort in anticipation of the very attractive physics possibilities. Overall, we concluded that the collaboration will be able to maintain the present level of manpower.

We are making an effort to induce some new groups to join our efforts. In addition, we are 'seeding' at other universities as SLD collaborators take professorial positions (e.g. Johns Hopkins and Oxford). We hope to have some modest success in this endeavor by using the argument that some SLD data analysis in the near future would be an attractive complement to getting involved in NLC detector R&D in the future.

We do believe, however, that the strength of the collaboration will be sufficient even without new groups to carry out the proposed run extension and complete the analysis and publication of the physics results from such an extension.

10 Computing

10.1 The Dominant Term: Monte Carlo

SLD continues to rely on Alpha/VMS for its compute cycles. The current computation capability is comprised of three facilities:

- $\sim$2500 specint92 Alpha farm (SLACVX cluster) which is primarily used for analysis and data processing. Secondarily, it has been used for MC generation.
- $\sim$1700 specint92 Alpha farm at Vanderbilt University. It is used solely for MC generation.
- $\sim$1000 specint92 AlphaServer owned by MCC; we have gleaned cycles from it parasitically for MC generation.

These facilities are capable of producing 18k, 18k and 12k hadronic Z MC events per day. Note that the SLACVX capacity assumes little or no concurrent analysis load.

It has been our experience that a generation cycle, in which a total of 10x the data sample is produced, should take no longer than three months. For the 350k Z's collected during the

1997-98 running period, it is believed that the installed capacity is close to sufficient. Work is in progress to bring a new facility online at Tohoku University, which would offset the analysis load on SLACVX.

We have found that we obtain approximately 10,000 events per day per 1000 specint92 of capacity. Consequently, a total data sample of 1 million Z's would necessitate an additional 100k events generated per day, which translates into 10k specint92.

Vanderbilt believes it can perform modest upgrades to their facility, which would increase their capacity by 15k events/day. They are attempting to get additional funds from DoE to further expand the farm. With an infusion of $\sim$\$13k, Tohoku could have an installed capacity of 1800 specints, producing about 20k events/day. This leaves a shortfall of 6.5k specints, presumably to be acquired at SLAC.

It is difficult to estimate pricing on compute hardware. We currently estimate that it would cost $\sim$\$220k to put 4.5k specints into the SLACVX AlphaServer 8400. The additional 2k specints could come from a used AlphaServer 4100 for a cost of between \$50-100k. Should the non-SLAC farms not be able to deliver the expected capacities, SLAC would be required to shore up the difference.

10.2 Additional Resources Required

SLD's *real time* data processing is controlled by a sophisticated server, which runs on SLAC's venerable IBM VM mainframe. This server is not portable and its author is no longer with SLD. SCS has decided to terminate VM immediately after the 97-98 run and to guarantee a replacement for the processing server. We may turn this into an opportunity to upgrade the data processing system, both in terms of streamlining and modernizing it.

SLD writes its data directly to the tape silo. This link must be maintained. In addition, 12 silo drives are attached to the SLACVX cluster via the 8400, using 3490 cartridges. We believe we have an ample supply of 3490 cartridges to handle the data and MC load.

Acknowledgments

We would like to thank our colleagues in the SLAC theory group for many useful discussions and suggestions.

References

[1] M. Woods, SLAC-PUB-7319, (1996). Refer also to the theses by E. Torrence, SLAC-Report-509 (1997); R. King, SLAC-Report-452 (1994); A. Lath, SLAC-Report-454 (1994); and R. Elia, SLAC-Report-429 (1994).

[2] M. Woods, SLAC-PUB-7320, (1996); and M. Woods, SLAC-PUB-6694 (1995).

[3] R.C. Field et al., OREXP 97-04 (1997).

[4] D. Onoprienko et al., UTKHEP-97-20 (1997).

[5] K. Abe *et al.*, Nucl. Inst. Meth. **A343** (1994) 74.

[6] T.J. Pavel, Ph. D. Thesis, Stanford University, SLAC-R-491 (1996).

[7] K. Abe et al., Nucl. Instr. and Meth. **A371** (1996) 195.

[8] K. Abe *et al.*, *Phys. Rev. Lett.* **70**, 2515 (1993); K. Abe *et al.*, *Phys. Rev. Lett.* **73**, 25 (1994) [hep-ex/9404001]; K. Abe *et al.*, **78**, 2075 (1997) [hep-ex/9611011].

[9] K. Abe *et al.*, *Phys. Rev. Lett.* **74**, 2880 (1995) [hep-ex/9410009]; K. Abe *et al.*, *Phys. Rev. Lett.* **79**, 804 (1997) [hep-ex/9704012].

[10] K. Abe *et al.*, *Phys. Rev. Lett.* **78**, 17 (1997) [hep-ex/9609019].

[11] See the talk of D. Karlen, 29^{th} International Conference on High-Energy Physics (ICHEP 98).

[12] M.E. Peskin and T. Takeuchi, *Phys. Rev. Lett.* **65**, 964 (1990), and *Phys. Rev.* **D46**, 381 (1992); W.J. Marciano and J.L. Rosner, *Phys. Rev. Lett.* **65**, 2963 (1990); D.C. Kennedy and P.G. Langacker, *Phys. Rev. Lett.* **65**, 2967 (1990); G. Altarelli, and R. Barbieri *Phys. Lett.* **B253**, 161 (1991) and G. Altarelli, R. Barbieri, and S. Jadach, *Nucl. Phys.* **B369**, 3 (1992).

[13] D.M. Pierce, J.A. Bagger, K. Matchev, and R-j. Zhang, *Nucl. Phys.* **B491**, 3 (1997).

[14] ZFITTER 5.10: D. Bardin, *et al.*, CERN-TH. 6443/92 (1992) [hep-ph/9412201].

[15] T. Takeuchi, A.K. Grant, and J.L. Rosner, FERMILAB-CONF-94-279-T, Aug 1994, hep-ph/9409211.

[16] M. Kobayashi and T. Maskawa, *Progr. Theor. Phys.* **49**, 652 (1973).

[17] A. Ali and D. London, *Z. Phys.* **C65**, 431 (1995).

[18] LEP B Oscillations Working Group, *Combined Results on B^0 Oscillations: Results for Summer 1998 Conferences*, LEPBOSC 98/3, July 1998.

[19] J.L. Hewitt, T. Takeuchi, and S. Thomas in *Electroweak Symmetry Breaking and New Physics at the TeV Scale*; ed. T. Barklow *et al.*, World Scientific, Singapore (1997).

[20] P. Paganini *et al.*, hep-ph/9711261, hep-ph/9802289, submitted to Physica Scripta.

[21] H.-G. Moser and A. Roussarie, *Nucl. Inst. and Meth.* **A384**, 491 (1997).

[22] M. Beneke, J. Buchalla, and I. Dunietz, *Phys. Rev.* **D54**, 4419 (1996).

[23] A.J. Buras, to appear in Proceedings, Symposium on Heavy Flavors, Santa Barbara, 1997.

[24] M. Bilenky, G. Rodrigo, A. Santamaria, Nucl. Phys. **B439** (1995) 505;
J. Fuster, S. Cabrera, S. Marti i Garcia, Nucl. Phys. (Proc. Suppl.) **54A** (1997) 39.

[25] T. G. Rizzo, Phys. Rev. **D50** 4478 (1994).

[26] K. Abe *et al.*, SLAC-PUB-7660 (1997); to be subm. to Phys. Rev. D.

[27] T. Rizzo, private communication (1996).

[28] K. Abe *et al.*, SLAC-PUB-7572 (1997).

[29] P. N. Burrows and P. Osland, Phys. Lett. **B400**, 385 (1997).

[30] K. Abe *et al.*, Phys. Rev. Lett. **75** (1995) 4173.

[31] A. Brandenburg, L. Dixon, and Y. Shadmi, Phys. Rev. **D53**, 1264 (1996).

[32] See, for example, C. D. Carone and H. Murayama, Phys. Rev. Lett. **74**, 3122 (1995).

[33] K. Abe *et al.*, SLAC-PUB-7570 (1997).

[34] K. Abe *et al.*, Phys. Rev. **D56** (1997) 5310.

[35] A. Bohrer, Phys. Rept. **291** (1997) 107.

[36] K. Abe, et al., SLAC-PUB-7766, to be submitted to Phys. Rev. D.

[37] K. Abe *et al.*, Phys. Rev. Lett. **78** (1997) 3442.

[38] K. Abe *et al.*, Phys. Rev. Lett. **74** (1995) 1512.

[39] K. Abe *et al.*, SLAC-PUB-7574 (1997).